# Characterization of Frictional Multi-Legged Equilibrium Postures on Uneven Terrains

**Yizhar Or*** **and Elon Rimon**
Dept. of Mechanical Engineering, Technion, Israel Inst. of Technology

**Abstract** *Quasistatic legged locomotion over uneven terrains requires characterization of the legged robot equilibrium postures as well as understanding of the non-static motion modes that can develop at the contacts. This paper characterizes the frictional multi-legged equilibrium postures on a generic class called* **tame stances***, which satisfy a generalized support polygon principle. To characterize the equilibrium postures, the paper lumps the legged mechanism's kinematic structure into a rigid body having a variable center of mass and maintaining the same contacts with the terrain. The equilibrium postures associated with a given set of contacts correspond to the center of mass locations at which the body is supported in static equilibrium by the same contacts under the influence of gravity. The paper thus characterizes the feasible equilibrium region of a rigid body having a variable center of mass and supported by multiple frictional contacts under the influence of gravity. The paper establishes that the feasible equilibrium region forms a convex set which has* five types *of boundary curves. These boundary curves are formulated analytically, illustrated with graphical examples, and associated with the onset of five non-static motion modes at the contacts. The paper also compares the analytical results against experimental measurements conducted on a legged mechanism prototype.*

## 1 Introduction

Developers of legged robots strive to achieve stable locomotion over increasingly more demanding terrains such as staircases (Hirai et al., 1998; Hirose et al., 2001; Kaneko et al., 2011), outdoor terrains (Murphy et al., 2011; Neuhaus et al., 2011; Rebula et al., 2007), planetary terrains (Bares and Wettergreen, 1999; Krotkov and Simmons, 1996; Wilcox et al., 2007), and disaster areas (Guizzo and Ackerman, 2012). All of these tasks involve quasistatic legged locomotion, where the robot moves through a series of legged postures while supporting itself in static equilibrium against gravity (Boissonnat et al., 2000; Goodwine and Burdick, 2002; Madhani and Dubowsky, 1992). To ensure *safe* quasistatic locomotion, we need tools to characterize which legged postures can stably support the mechanism against gravity on uneven terrains. This paper characterizes the legged equilibrium postures on a generic class of uneven terrains which satisfies a generalized support polygon principle. For any given set of frictional contacts, the paper characterizes the *feasible equilibrium region* where the legged mechanism can vary its center of mass while maintaining its static equilibrium posture, and also identifies the non-static motion modes that can develop once the center of mass crosses the boundary of the feasible equilibrium region.

The robotics literature on quasistatic legged locomotion started with the works of Orin (Marhefka and Orin, 1997) and Mcghee (McGhee and Frank, 1968), who refer to static equilibrium postures as *statically stable* postures. More recent legged locomotion papers discuss the static stability of humanoid robots (Hirai et al., 1998; Kaneko et al., 2011; Yokokohji et al., 2002) as well as quadruped robots (Murphy et al., 2011; Neuhaus et al., 2011; Rebula et al., 2007). When considering the static stability of legged robots, a leading concept is the *support polygon principle* (Loc et al., 2012; McGhee and Frank, 1968; McGhee and Iswandhi, 1979). It states that on a flat horizontal terrain, the legged mechanism's center of mass must lie in the vertical prism whose cross section is the convex polygon spanned by the contacts supporting the mechanism against gravity. This principle was extended for dynamic motion synthesis of legged robots (Kuffner et al., 2001; Sugihara and Nakamura, 2003) with the concept of *zero moment point* (ZMP) (Vukobratovic and Borovac, 2004; Yokoi et al., 2004; Shin and Kim, 2014). However, the support polygon and ZMP principles apply only to *flat horizontal terrains* (although some ZMP extensions to uneven terrains have been investigated (Park and Youm, 2007; Sentis et al., 2011; Takubo et al., 2009)).

One expects that the grasping literature will provide useful insight for the problem discussed in this paper. However, a typical grasping system differs from a legged robot system in two fundamental ways. First, the condition of *force closure* in grasping systems captures the fingers' ability to resist any external

*Corresponding author: Dept. of ME, Technion, Haifa, Israel 32000, izi@tx.technion.ac.il.

wrench that may act on the grasped object (Liu et al., 2002; Nguyen, 1988; Xu et al., 2004). In contrast, legged postures are typically *not* force closure, as the ground contacts can resist only a specific set of external wrenches that act on the legged robot (Hong and Cipra, 2006). Second, a typical grasping system assumes *full control* of the finger contact forces (Fen et al., 1996; Schlegl et al., 2001). In contrast, legged robots can generate only passive reaction forces at the ground contacts. In this sense quasistatic legged locomotion is more closely related to non-prehensile object manipulation (Blind et al., 2001; Erdmann, 1998; Lynch and Mason, 1996) as well as whole arm object manipulation (Mirza and Orin, 1994; Omata and Nagata, 2000; Park et al., 2001). The grasping literature provides a computational approach which formulates the frictional equilibrium constraints as a linear matrix inequality (LMI) problem (Han et al., 2000). Importantly, LMI and other convex optimization techniques can only answer a feasibility query on a given point, or provide extremal values of *a scalar function*. Thus, these methods can only be used to find discrete boundary points of the feasible equilibrium region along a specific ray. In the context of quasistatic locomotion, computing the center of mass feasible equilibrium region reduces to finding the *projection* of a high-dimensional convex cone on a plane (Bretl and Lall, 2008). Since the exact computation of this projection is highly complicated, Bretl proposed a method that computes polygonal inner and outer approximations for this projection (Bretl and Lall, 2006, 2008). These methods have been used to construct an algorithmic motion planner for multi-legged robots (Hauser et al., 2008). Recent works (Caron et al., 2015; Prete et al., 2016) have used similar principles for generating fast and computationally-efficient planning algorithms, while the nonlinear friction constraints were replaced by polyhedral approximations. Nevertheless, these numerical procedures do not provide any analytic characterization or physical insight concerning the boundary of the feasible equilibrium region.

In order to characterize the statically stable postures of a legged mechanism, its kinematic structure is lumped into a rigid body having a variable center of mass and maintaining the same contacts with the terrain. The legged mechanism's feasible equilibrium postures associated with a given set of frictional contacts correspond to the center of mass locations at which the body is supported in static equilibrium by the same contacts under the influence of gravity. The paper thus characterizes the exact *feasible equilibrium region* associated with a given set of frictional contacts, defined as all center of mass locations at which the terrain's contact forces can balance the gravitational wrench (i.e. force and torque) acting on the rigid body. The paper additionally describes which non-static motion modes will develop at the contacts when the center of mass crosses the boundary of the feasible equilibrium region. The paper complements the analytic results with computational examples, which are compared against experimental measurements of the five types of boundary curves. The paper completes our earlier work which was limited to feasible equilibrium region of three-legged tame stances (Or and Rimon, 2010). The current paper generalizes the notion of tame stances, where the contact arrangement is not too steep, to the case of multiple contacts. Then it presents characterization and computation of all possible types of boundary curves for any number of frictional contacts.

The paper is structured as follows. Section 2 defines the feasible equilibrium region of a legged mechanism and introduces the class of tame stances. Sections 3 and 4 describe a general scheme under which the feasible equilibrium region is characterized. Section 5 gives a detailed geometric and analytic characterization of all five types of boundary curves of the feasible equilibrium region over uneven tame stances. Section 6 describes computational examples of the feasible equilibrium region associated with three, four, and five-legged postures. These examples are then experimentally verified in Section 7. The concluding section discusses extension of the results to non-tame stances, which no longer satisfy any generalized support polygon principle. The supplementary material contains proofs of results stated throughout the paper, as well as MATLAB code files which compute the feasible equilibrium region of a given legged posture.

# 2 The Feasible Equilibrium Region of Tame Stances

This section defines the feasible equilibrium region associated with $k$ supporting contacts, the notion of *tame stances* over uneven terrains, and the generalized support polygon principle satisfied by these stances.

## 2.1 Definition of the Feasible Equilibrium Region

When a legged robot is supported by a given set of frictional contacts, the mechanism's kinematic structure can be lumped into a 3D rigid body, $\mathcal{B}$, having a variable center of mass and supported by the same contacts against gravity. In order to characterize the legged mechanism's statically stable equilibrium postures, one can equivalently characterize the body's center of mass positions, termed the *feasible equilibrium region,* at which the supporting contacts can resist the gravitational wrench acting on $\mathcal{B}$. The supporting contacts

are located at $x_1 \dots x_k \in I\!R^3$, and they are modeled as *hard-point contacts* which generate negligible torque about the contact normals (Mason and Salisbury, 1985). The contact forces are denoted $f_1, \dots, f_k \in I\!R^3$. The position of $\mathcal{B}$'s center of mass is denoted $\boldsymbol{x}_c \in I\!R^3$, and the gravitational force acting on $\mathcal{B}$ at $\boldsymbol{x}_c$ is denoted $f_g$. We use the standard basis for $I\!R^3$, such that $\boldsymbol{e} = (0,0,1)$ is the upward vertical direction collinear with $f_g$. The horizontal basis vectors form the rows of the *projection matrix*, $\mathbf{E} = \begin{pmatrix} 1 & 0 & 0 \\ 0 & 1 & 0 \end{pmatrix}$, which projects vectors in $I\!R^3$ to the horizontal plane. The horizontal projection of the contact points, contact forces, and center of mass position are denoted $\tilde{x}_i = \mathbf{E}x_i$, $\tilde{f}_i = \mathbf{E}f_i$ and $\tilde{\boldsymbol{x}}_c = \mathbf{E}\boldsymbol{x}_c$, respectively. Assuming Coulomb's friction model, the contact reaction forces must lie in their respective friction cones:

$$C_i = \left\{ f_i \in I\!R^3 : f_i \cdot n_i \geq 0 \text{ and } \sqrt{(f_i \cdot s_i)^2 + (f_i \cdot t_i)^2} \leq \mu_i \, |f_i \cdot n_i| \right\} \quad i = 1 \dots k \tag{1}$$

where $\mu_i$ is the coefficient of friction at $x_i$, $n_i$ is the terrain's outward unit normal at $x_i$, and $(s_i, t_i)$ are the terrain's unit tangents at $x_i$ such that $(s_i, t_i, n_i)$ forms a right-handed frame. The body $\mathcal{B}$ is supported at a *feasible equilibrium stance* when permissible contact forces can balance the gravitational wrench, as stated in the following definition.

**Definition 1.** *A* **k-contact equilibrium stance** *of $\mathcal{B}$ satisfies the condition:*

$$\begin{pmatrix} f_1 \\ x_1 \times f_1 \end{pmatrix} + \dots + \begin{pmatrix} f_k \\ x_k \times f_k \end{pmatrix} = - \begin{pmatrix} f_g \\ \boldsymbol{x}_c \times f_g \end{pmatrix} \qquad f_i \in C_i \text{ for } i = 1 \dots k \tag{2}$$

*where $(f_i, x_i \times f_i) \in I\!R^6$ is the wrench (i.e. force and torque) generated by $f_i$ for $i = 1 \dots k$, and $(f_g, \boldsymbol{x}_c \times f_g) \in I\!R^6$ is the wrench generated by the gravitational force $f_g$.*

Note that the term *stance* implies the presence of gravity. Hence a feasible equilibrium stance is a state of equilibrium under gravity. When the body $\mathcal{B}$ is supported by $k \geq 3$ frictional contacts with center of mass at $\boldsymbol{x}_c$, the contact forces solving (2) generically vary in a $(3k-6)$-dimensional affine space in $I\!R^{3k}$. The feasible equilibrium region associated with a given set of frictional contacts is defined as follows.

**Definition 2** ((Or and Rimon, 2010))**.** *Let a 3D rigid body $\mathcal{B}$ be supported by frictional contacts $x_1, \dots, x_k$ with coefficients of friction $\mu_1, \dots, \mu_k$ under the influence of gravity. The* **feasible equilibrium region,** *$\mathcal{R} \subseteq I\!R^3$, is the set of all $\mathcal{B}$'s center of mass positions $\boldsymbol{x}_c$ at which there exist feasible contact reaction forces, $f_i \in C_i$ for $i = 1 \dots k$, satisfying the equilibrium stance condition* (2)*.*

The following proposition reviews a generic property of the feasible equilibrium region over general uneven terrains (Or and Rimon, 2010).

**Proposition 2.1** ((Or and Rimon, 2010))**.** *Let a rigid body $\mathcal{B}$ be supported by k frictional contacts against gravity. If the feasible equilibrium region, $\mathcal{R}$, is nonempty, it is a vertical line for a single contact, a vertical strip for two contacts, and generically a* **vertical cylindrical set with a convex cross-section** *for $k \geq 3$ contacts.*

## 2.2 The Class of Tame Stances

Since $\mathcal{R}$ forms a convex set of vertical lines in $I\!R^3$, its computation reduces to the computation of its *horizontal cross-section*, denoted $\widetilde{\mathcal{R}}$, in $I\!R^2$. From this point onward, we will refer to the horizontal cross-section of $\mathcal{R}$, $\widetilde{\mathcal{R}} \subset I\!R^2$, as the *feasible equilibrium region* of the given stance. When computing equilibrium postures on flat horizontal terrains, a classical concept is the following support polygon principle.

**Definition 3** ((Or and Rimon, 2010))**.** *The* **support polygon** *associated with frictional contacts $x_1, \dots, x_k$ is the horizontal polygon, $\mathcal{P} \subset I\!R^2$, spanned by the horizontal projection of the contact points, $\mathcal{P} = \mathsf{conv}\{\tilde{x}_1, \dots, \tilde{x}_k\}$, where* conv *is the convex hull of the given set of points.*

The support polygon forms a convex set bounded by a closed loop of line segments connecting projected contact pairs $(\tilde{x}_i, \tilde{x}_j)$ (note that not all contact points necessarily contribute to the boundary $\mathcal{P}$). While $\widetilde{\mathcal{R}} = \mathcal{P}$ on flat horizontal terrains, the relation between $\widetilde{\mathcal{R}}$ and $\mathcal{P}$ is rather complex on *uneven* terrains. A large class of stances on uneven terrains satisfies the relation $\widetilde{\mathcal{R}} \subseteq \mathcal{P}$, and this class is next defined.

**Definition 4** (**Tame Stances**)**.** *A k-contact stance is* **tame** *if for each pair of contacts $x_i, x_j$, the friction cone at every contact $x_p$, $C_p$ for $p \neq i, j$, lies above the line segment $(x_i, x_j)$:*

$$\forall f_p \in C_p \qquad \boldsymbol{n}_{ijp} \cdot f_p \geq 0 \qquad p = 1 \dots k \text{ such that } p \neq i, j$$

*where $\boldsymbol{n}_{ijp}$ is the vector normal to the plane spanned by $x_i$, $x_j$, and $x_p$, such that $\boldsymbol{n}_{ijp} \cdot \boldsymbol{e} \geq 0$.*

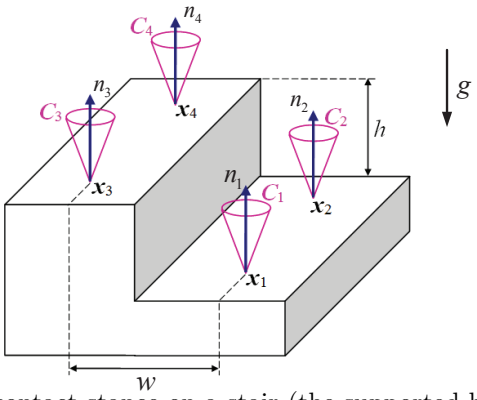

Figure 1: A four-contact stance on a stair (the supported body is not shown).

The definition is a direct generalization of the notion of 3-contact tame stances defined in (Or and Rimon, 2010). Geometrically, it requires that the contacts' slopes and height differences are not too steep. In order to describe the generalized support polygon principle satisfied by tame stances, define a contact $x_i$ with friction cone $C_i$ as *quasi-flat* when $\boldsymbol{e} \in C_i$, where $\boldsymbol{e}$ is the upward vertical direction in $\mathbb{R}^3$. A $k$-contact stance is said to be *quasi-flat* when its $k$ contacts are all quasi-flat ((Or and Rimon, 2010; Prete et al., 2016)). The following proposition summarizes the relations between $\widetilde{\mathcal{R}}$ and $\mathcal{P}$.

**Proposition 2.2.** *The feasible equilibrium region of a tame $k$-contact stance, $\widetilde{\mathcal{R}}$, is* **fully contained** *in the support polygon, $\widetilde{\mathcal{R}} \subseteq \mathcal{P}$. The converse relationship, $\mathcal{P} \subseteq \widetilde{\mathcal{R}}$, always holds for quasi-flat stances.*

The Proof of this proposition, which is a direct extension of a result from (Or and Rimon, 2010), appears in the supplementary document. The main idea behind the proof of $\widetilde{\mathcal{R}} \subseteq \mathcal{P}$ is the fact that for every two contacts $x_i, x_j$ that contribute to the boundary of $\mathcal{P}$, the requirement of tame stance implies that the gravitational torque can be balanced only if $\boldsymbol{x}_c$ lies a halfspace of $\mathbb{R}^3$ which is bounded by the vertical plane passing $x_i$ and $x_j$. Proposition 2.2 implies that $\widetilde{\mathcal{R}} = \mathcal{P}$ for tame stances with quasi-flat contacts. For instance, $\widetilde{\mathcal{R}} = \mathcal{P}$ holds on flat horizontal terrains. Uneven terrains with quasi-flat contacts remain tame as long as the terrain is not too steep, as demonstrated in the following example.

**Example:** Consider the four-contact stance on a stair depicted in Figure 1. On such horizontal supports $n_i = \boldsymbol{e}$ for $i = 1 \ldots 4$, hence all contacts are quasi-flat. As long as the stair forms a tame stance the feasible equilibrium region satisfies the equality $\widetilde{\mathcal{R}} = \mathcal{P}$. To determine which stairs form tame stances, assume a uniform coefficient of friction $\mu$ at the contacts. Denote by $h$ the stair's vertical height and by $w$ the stair's horizontal width. The stair becomes steeper as $h$ is increased while $w$ is kept constant, and remains tame as long as $h \leq w/\mu$. For instance, a stair with $w = 30$ cm and coefficient of friction $\mu = 0.4$ remains tame for stair heights satisfying $h \leq 75$ cm. For a higher step with $h > 75$ cm, the feasible equilibrium region exceeds beyond the support polygon, $\widetilde{\mathcal{R}} \supset \mathcal{P}$. ○

On general uneven terrains some or all contacts may not be quasi-flat. On such terrains the classical support polygon principle *can no longer be safely used* to choose statically stable equilibrium postures, since $\widetilde{\mathcal{R}}$ forms a strict subset of $\mathcal{P}$ on such terrains. Safe quasistatic locomotion therefore requires explicit characterization of the more complex region $\widetilde{\mathcal{R}}$, which is the paper's main contribution.

# 3 A Scheme for Computing the Feasible Equilibrium Region of K-Contact Stances

This section describes a scheme for computing the feasible equilibrium region of a rigid body $\mathcal{B}$ supported by a given set of frictional contacts $x_1, \ldots, x_k$. Generalized from (Or and Rimon, 2010), this scheme is based on a geometric interpretation of the equilibrium equation (2), which lives in $\mathcal{B}$'s six-dimensional *wrench space* of forces and torques, $\boldsymbol{w} = (f, \tau) \in \mathbb{R}^6$. The left side of (2) represents the net wrench generated by the contact forces $f_1, \ldots, f_k$. Each contact force $f_i$ is restricted to lie within its convex friction cone, $C_i$, defined in (1). The set of all net wrenches that can be possibly generated by a given set of frictional contacts is defined as follows.

**Definition 5.** *Let a rigid body $\mathcal{B}$ be supported by $k$ frictional contacts in $\mathbb{R}^3$. The* **net wrench cone** *of a $k$-contact stance is the set of all net wrenches that can be affected on $\mathcal{B}$ by the supporting contacts:*

$$\mathcal{W} = \left\{ \sum_{i=1}^{k} \begin{pmatrix} f_i \\ x_i \times f_i \end{pmatrix} \in \mathbb{R}^6 : f_i \in C_i \text{ for } i = 1 \ldots k \right\} \tag{3}$$

*where $C_1, \ldots, C_k$ are the friction cones at the contacts $x_1, \ldots, x_k$.*

When a rigid body $\mathcal{B}$ is supported by $k \geq 3$ frictional contacts, $\mathcal{W}$ generically forms a *six-dimensional convex cone* in $\mathcal{B}$'s wrench space. A special case occurs when all $k \geq 3$ contacts are aligned along a common line in $\mathbb{R}^3$. In this case $\mathcal{W}$ degenerates into a five-dimensional convex cone in $\mathbb{R}^6$. Next consider the right side of the equilibrium equation (2). When $\mathcal{B}$'s center of mass varies in $\mathbb{R}^3$ while the body is supported by a given set of contacts, the horizontal projection of the body's center of mass, $\tilde{\boldsymbol{x}}_c$, determines the gravitational wrench acting on $\mathcal{B}$. It follows that the right side of (2) spans an *affine plane* in $\mathcal{B}$'s wrench space, defined as follows.

**Definition 6.** *The* **affine plane** *of gravitational wrenches generated by varying $\mathcal{B}$'s center of mass in $\mathbb{R}^3$ is given by*

$$L = \left\{ \begin{pmatrix} f \\ \tau \end{pmatrix} \in \mathbb{R}^6 : f = f_g \quad \textit{and} \quad f \cdot \tau = 0 \right\} \tag{4}$$

*where $f_g$ is the gravitational force acting on $\mathcal{B}$.*

Note that $f_g$ is a constant vertical force, hence (4) specifies four linear equations in the variable $(f, \tau) \in \mathbb{R}^6$. The gravitational torque affecting $\mathcal{B}$ is given by $\tau = \boldsymbol{x}_c \times f_g$. It follows that any wrench $(f, \tau) \in L$ corresponds to a *unique* horizontal center of mass position, $\tilde{\boldsymbol{x}}_c$. To obtain a formula for $\tilde{\boldsymbol{x}}_c$ as a function of $(f, \tau) \in L$, assume that $\|f_g\| = 1$ (this choice amounts to a choice of force units and has no influence on the generality of the results). Then $f_g = -\boldsymbol{e}$, and the triple vector product identity $\boldsymbol{e} \times \tau = -\boldsymbol{e} \times (\boldsymbol{x}_c \times \boldsymbol{e}) = -(\boldsymbol{x}_c - (\boldsymbol{x}_c \cdot \boldsymbol{e})\boldsymbol{e})$ gives the formula:

$$\tilde{\boldsymbol{x}}_c = -\mathbf{E}(\boldsymbol{e} \times \tau) \qquad \mathbf{E} = \begin{pmatrix} 1 & 0 & 0 \\ 0 & 1 & 0 \end{pmatrix}. \tag{5}$$

The following theorem specifies a scheme for constructing the feasible region $\widetilde{\mathcal{R}}$ in terms of the net wrench cone $\mathcal{W}$ and the affine plane $L$.

**Theorem 1.** *Let a rigid body $\mathcal{B}$ be supported by $k$ frictional contacts against gravity. The* **feasible equilibrium region** *of the $k$-contact stance is given by*

$$\widetilde{\mathcal{R}} = \left\{ \tilde{\boldsymbol{x}}_c \in \mathbb{R}^2 : \tilde{\boldsymbol{x}}_c = -\mathbf{E}(\boldsymbol{e} \times \tau) \;\; \textit{such that} \;\; \begin{pmatrix} -\boldsymbol{e} \\ \tau \end{pmatrix} \in \mathcal{W} \cap L \;\; \textit{in} \;\; \mathbb{R}^6 \right\} \tag{6}$$

*where $\mathcal{W}$ is the net wrench cone of the stance and $L$ is the affine plane of gravitational wrenches, both defined in (3) and (4). The* **boundary** *of $\widetilde{\mathcal{R}}$ is given by*

$$\mathsf{bdy}(\widetilde{\mathcal{R}}) = \left\{ \tilde{\boldsymbol{x}}_c \in \mathbb{R}^2 : \tilde{\boldsymbol{x}}_c = -\mathbf{E}(\boldsymbol{e} \times \tau) \;\; \textit{such that} \;\; \begin{pmatrix} -\boldsymbol{e} \\ \tau \end{pmatrix} \in \mathsf{bdy}(\mathcal{W}) \cap L \;\; \textit{in} \;\; \mathbb{R}^6 \right\} \tag{7}$$

*where $\mathsf{bdy}(\mathcal{W})$ is the five-dimensional boundary of the net wrench cone $\mathcal{W}$ in $\mathbb{R}^6$.*

**Proof:** Based on the geometric interpretation of the equilibrium equation (2), every wrench $(f, \tau) \in \mathcal{W} \cap L$ corresponds to a unique horizontal center of mass location, $\tilde{\boldsymbol{x}}_c = -\mathbf{E}(\boldsymbol{e} \times \tau)$. This gives formula (6). The projection matrix $\mathbf{E}$ can be interpreted as a linear map, $\mathbf{E} : L \to \mathbb{R}^2$, mapping the set $\mathcal{W} \cap L$ onto $\widetilde{\mathcal{R}}$. Being a non-singular linear map, it maps the interior of $\mathcal{W} \cap L$ to the interior of $\widetilde{\mathcal{R}}$, and the boundary of $\mathcal{W} \cap L$ to the boundary of $\widetilde{\mathcal{R}}$. The boundary of $\mathcal{W} \cap L$ within the affine plane $L$ consists of boundary points of $\mathcal{W}$ in $\mathbb{R}^6$. Hence the mapping of $\mathsf{bdy}(\mathcal{W}) \cap L$ under $\mathbf{E}$ gives the boundary of $\widetilde{\mathcal{R}}$. □

Based on Theorem 1, the boundary of the feasible equilibrium region, $\mathsf{bdy}(\mathcal{W})$, will be characterized in Section 4. Then in Section 5, the intersection $\mathsf{bdy}(\mathcal{W}) \cap L$ will be computed in $\mathcal{B}$'s wrench space and mapped by linear map (5) to the boundary of the feasible equilibrium region $\widetilde{\mathcal{R}}$.

# 4 The Boundary of the Net Wrench Cone of K-Contact Stances

This section characterizes the boundary of the net wrench cone, $\mathsf{bdy}(\mathcal{W})$, associated with $k \geq 3$ frictional contacts. First the space of contact forces $f_1, \ldots, f_k$ will be divided into cells. Next the cells that possibly contribute five-dimensional pieces of net wrenches to $\mathsf{bdy}(\mathcal{W})$ will be identified. Then the *critical contact forces* in the cells that contribute to $\mathsf{bdy}(\mathcal{W})$ will be analytically described.

## 4.1 Cellular Decomposition of the Contact Forces at a K-Contact Stance

The analysis is based on an interpretation of $\mathcal{W}$ as the image of the terrain's contact reaction forces under a linear map, $\mathcal{L}$, which gives the net wrench affected on $\mathcal{B}$ by these forces.[1] The domain of $\mathcal{L}$ is the space of all contacts forces $(f_1, \ldots, f_k) \in \mathbb{R}^{3k}$. Within this domain lies the *product set* $C_1 \times \cdots \times C_k$, consisting of all contacts forces $(f_1, \ldots, f_k)$ such that $f_i \in C_i$ for $i = 1 \ldots k$. The net wrench cone $\mathcal{W}$ is the image of $C_1 \times \cdots \times C_k$ under the linear map $\mathcal{L} : \mathbb{R}^{3k} \to \mathbb{R}^6$,

$$\mathcal{L}(f_1, \ldots f_k) = \textstyle\sum_{i=1}^{k} \begin{pmatrix} f_i \\ x_i \times f_i \end{pmatrix} \qquad \text{where } (f_1, \ldots, f_k) \in C_1 \times \cdots \times C_k. \tag{8}$$

[1] When an object $\mathcal{B}$ is held by a multi-finger hand, $\mathcal{L}$ is known as the *grasp map*.

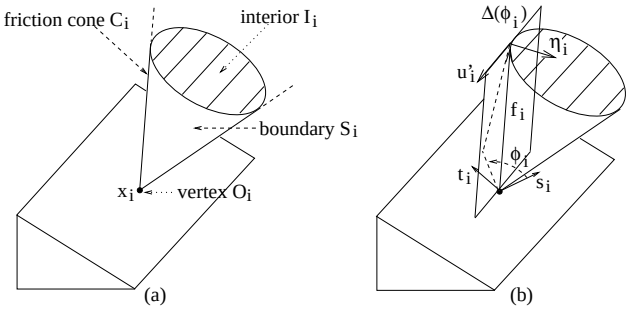


Figure 2: (a) Partition of the friction cone $C_i$ into its vertex $O_i$, punctured boundary $S_i$, and interior $I_i$. (b) The plane $\Delta_i(\phi_i)$ tangent to $S_i$ along a ray which starts at $x_i$ along the contact force $f_i = \lambda_i \boldsymbol{u}_i(\phi_i)$.

In order to find critical forces that map to the boundary $\mathcal{W}$, one must first undertand the structure of the product set $C_1 \times \cdots \times C_k$, which forms a *stratified set* in $\mathbb{R}^{3k}$. That is, a set that can be decomposed into disjoint *cells,* each being a manifold without boundary. The cells' dimension ranges between zero (a single point manifold), and $3k$ (an open set in the ambient $\mathbb{R}^{3k}$). In order to describe how $C_1 \times \cdots \times C_k$ decomposes into cells, consider the decomposition of each friction cone into three subsets depicted in Figure 2(a):

$$C_i = O_i \cup I_i \cup S_i \qquad i = 1 \ldots k$$

where $O_i = \{0\}$ is the cone's vertex point, $I_i$ is the cone's interior, and $S_i$ is the cone's boundary surface excluding its vertex point (note that $I_i$ and $S_i$ contain only non-zero forces). Using this notation, the set $C_1 \times \cdots \times C_k$ can be decomposed into $3^k$ cells given by

$$C = (O_1 \cup I_1 \cup S_1) \times \cdots \times (O_k \cup I_k \cup S_k). \tag{9}$$

Each cell in $C_1 \times \cdots \times C_k$ represents a choice of one component from $\{O_i, I_i, S_i\}$ for $i = 1 \ldots k$. The dimension of any particular cell equals the *sum* of its component cell dimensions. For instance, the cell $O_1 \times S_2 \times S_3$ is four-dimensional, since $O_1$ is zero-dimensional while $S_2$ and $S_3$ are two-dimensional surfaces. Also note that $O_1 \times \cdots \times O_k$ is a zero-dimensional cell (a single point manifold), while $I_1 \times \cdots \times I_k$ is a $3k$-dimensional cell (an open set in the ambient $\mathbb{R}^{3k}$).

## 4.2 The Contact Force Cells That Contribute to the Boundary of $\mathcal{W}$

The boundary of the net wrench cone forms a five-dimensional set in $\mathcal{B}$'s wrench space (which is equivalent to $\mathbb{R}^6$). This set can be stratified into cells of dimension ranging between zero and five. The boundary of $\mathcal{W}$ is thus *fully captured* by the union of its five-dimensional cells, as cells of lower dimension can be obtained by intersecting two or more five-dimensional boundary cells. Let us therefore focus on characterizing the five-dimensional boundary cells of $\mathcal{W}$, based on the following criterion.

**Lemma 4.1.** *Let $\mathcal{K}$ be a cell of the set $C_1 \times \cdots \times C_k$. If the image of $\mathcal{K}$ under $\mathcal{L}$ contains a five-dimensional boundary cell of the net wrench cone $\mathcal{W}$, the boundary cell must be the image of* **critical contact forces** *in $\mathcal{K}$ satisfying the condition:*

$$\mathsf{rank}(\mathsf{D}\mathcal{L}_\mathcal{K}) = 5, \tag{10}$$

*where $D\mathcal{L}_\mathcal{K}$ is the Jacobian of the restriction of the map $\mathcal{L} : \mathbb{R}^{3k} \to \mathbb{R}^6$ to the cell $\mathcal{K}$.*

**Proof sketch:** When $\mathcal{K}$ is a five-dimensional cell, the condition $\mathsf{rank}(\mathsf{D}\mathcal{L}_\mathcal{K}) = 5$ ensures that the entire cell is mapped by $\mathcal{L}$ to a five-dimensional set in $\mathbb{R}^6$ that can possibly lie on the boundary of $\mathcal{W}$. When $\mathcal{K}$ has dimension six or higher, points where the Jacobian has full rank, $\mathsf{rank}(\mathsf{D}\mathcal{L}_\mathcal{K}) = 6$, are mapped by $\mathcal{L}$ into the interior of $\mathcal{W}$ according to the inverse function theorem (Guillemin and Pollack, 1974). Hence only points where $\mathsf{rank}(\mathsf{D}\mathcal{L}_\mathcal{K}) \leq 5$ are possibly mapped to the boundary of $\mathcal{W}$. Points where $\mathsf{rank}(\mathsf{D}\mathcal{L}_\mathcal{K}) = 5$ generically form a five-dimensional subset of $\mathcal{K}$, based on the following argument. When a cell $\mathcal{K}$ has dimension $d \geq 6$, points where $\mathsf{rank}(\mathsf{D}\mathcal{L}_\mathcal{K}) = 5$ can be described by zero determinant of $d$–5 six-column subsets of $D\mathcal{L}_\mathcal{K}$. This gives $d$–5 equations whose solution generically forms a five-dimensional set in $\mathcal{K} \cong \mathbb{R}^d$. Based on a similar argument, points in $\mathcal{K}$ where $\mathsf{rank}(\mathsf{D}\mathcal{L}_\mathcal{K}) < 5$ satisfy higher numbers of equations and generically form lower dimensional subsets of $\mathcal{K}$. Thus, only critical contact forces satisfying condition (10) are possibly mapped under $\mathcal{L}$ to five-dimensional boundary cells of $\mathcal{W}$. □

Lemma 4.1 specifies a necessary condition under which a cell $\mathcal{K}$ contributes a five-dimensional cell to the boundary of $\mathcal{W}$. To apply Lemma 4.1, one must choose a parametrization for each cell $\mathcal{K}$ of dimension $d$, formulate the restricted map $\mathcal{L}_\mathcal{K}$ in terms of the chosen $d$ parameters, then compute the Jacobian matrix $D\mathcal{L}_\mathcal{K} \in \mathbb{R}^{6 \times d}$ and find conditions for its rank deficiency. A cell $\mathcal{K}$ can be assigned $d$ parameters according to its $S_i$ and $I_i$ components as follows. The contact forces lying in the friction cone interior, $I_i$, are simply parametrized by their cartesian coordinates: $f_i \in \mathbb{R}^3$, where the components of $f_i$ are expressed in a reference frame $(s_i, t_i, n_i)$ based at $x_i$. The contact forces on the friction cone boundary, $S_i$, are parametrized by

$(\lambda_i, \phi_i) \in \mathbb{R}^+ \times \mathbb{R}$, where $\lambda_i > 0$ is the force magnitude and $\phi_i$ is the force angle, measured by projecting $f_i$ on the terrain's $(s_i, t_i)$ tangent plane at $x_i$ (Figure 2(b)). The forces $f_i \in S_i$ are thus parametrized by

$$f_i(\lambda_i, \phi_i) = \lambda_i \boldsymbol{u}_i(\phi_i) \quad \text{such that} \quad \boldsymbol{u}_i(\phi_i) = \mu_i \cos(\phi_i)\boldsymbol{s}_i + \mu_i \sin(\phi_i)\boldsymbol{t}_i + \boldsymbol{n}_i \tag{11}$$

Where $\mu_i$ is the coefficient of friction at $x_i$. Since $\boldsymbol{u}_i(\phi_i)$ has a constant magnitude, $\boldsymbol{u}_i'(\phi_i) = -\mu_i \sin(\phi_i)\boldsymbol{s}_i + \mu_i \cos(\phi_i)\boldsymbol{t}_i$ is orthogonal to $\boldsymbol{u}_i(\phi_i)$. The pair $\{\boldsymbol{u}_i(\phi_i), \boldsymbol{u}_i'(\phi_i)\}$ thus spans the *tangent plane* to $S_i$ at the point $f_i(\lambda_i, \phi_i) \in S_i$, which will be denoted $\Delta_i(\phi_i)$ (Figure 2(b)). Note that $\Delta_i(\phi_i)$ is tangent to $S_i$ along a ray which starts at $x_i$. Finally, the vector $\boldsymbol{\eta}_i(\phi_i) = \boldsymbol{u}_i(\phi_i) \times \boldsymbol{u}_i'(\phi_i) = -\mu_i \cos(\phi_i)\boldsymbol{s}_i - \mu_i \sin(\phi_i)\boldsymbol{t}_i - \mu_i^2 \boldsymbol{n}_i$ is *normal* to $S_i$ at the point $f_i(\lambda_i, \phi_i) \in S_i$, as shown in Figure 2(b). The cells of $C_1 \times \cdots \times C_k$ are next partitioned into *cell classes* as follows.

**Definition 7.** *Each* **cell class** *in the set $C_1 \times \cdots \times C_k = (O_1 \cup I_1 \cup S_1) \times \cdots \times (O_k \cup I_k \cup S_k)$ is associated with $n_S$ choices of $S_i$ components, $n_I$ choices of $I_i$ components, and $k - n_S - n_I$ choices of $O_i$ components which represent zero contact forces.*

Each cell class in $C_1 \times \cdots \times C_k$ can be represented by a formal word of $k$ letters from the alphabet $\{S, I, O\}$, having $n_S$ letters $S$, $n_I$ letters $I$, and $k - n_S - n_I$ letters $O$. For notational simplicity, we will use the convention that contact forces with indices $1 \ldots n_S$ lie in the boundary components $S_i$, contact forces with indices $n_S + 1 \ldots n_S + n_I$ lie in the interior components $I_i$, while the remaining contact forces with indices $n_S + n_I + 1 \ldots k$ are zero forces. This arbitrary choice of contact ordering will represent all other possible permutations of the contact indices for any given cell class. For instance, for $k = 3$ contacts the cell class $SIO$ represents six cells: $S_1 \times I_2 \times O_3$, $S_1 \times O_2 \times I_3$, $O_1 \times S_2 \times I_3$, $O_1 \times I_2 \times S_3$, $I_1 \times O_2 \times S_3$, and $I_1 \times S_2 \times O_3$. In the following analysis, the letters $O$ will be omitted. For instance, the cell class $SIO$ will be denoted as $SI$. Note that all cells of a given class have the same dimension, given by $2n_S + 3n_I$. For instance, for $k = 3$ contacts all cell classes of dimension five or higher are: $SI$, $II$, $SSS$, $SSI$, $SII$, and $III$.

The following theorem lists all the cell classes in $C_1 \times \cdots \times C_k$ that can possibly contribute five-dimensional pieces to the boundary of the net wrench cone $\mathcal{W}$ at a tame $k$-contact stance. A $k$-contact stance is considered *generic* when the contacts do not lie on a common line in $\mathbb{R}^3$.

**Theorem 2** (**Boundary Cell Classes**). *The cell classes in $C_1 \times \cdots \times C_k$ whose image under $\mathcal{L}$ possibly contributes* **five-dimensional boundary pieces** *to the net wrench cone $\mathcal{W}$ at a generic tame $k$-contact stance are $SI$, $II$, $SSI$, $SSS$, $SSSS$, and $SSSSS$.*

The proof of Theorem 2 appears in the supplementary document. The proof verifies that the Jacobian matrix, $D\mathcal{L}_\mathcal{K}$, has *full rank* on each cell class of $C_1 \times \cdots \times C_k$ excluded from Theorem 2. When $D\mathcal{L}_\mathcal{K}$ has full rank on a cell $\mathcal{K}$ of dimension six or higher, the cell is mapped into the interior of $\mathcal{W}$ in $\mathbb{R}^6$. For instance, consider the $III$ and $SII$ cell classes. In the $III$ cell class, $D\mathcal{L}_\mathcal{K}$ has full rank when the contacts do not lie on a common line in $\mathbb{R}^3$. In the $SII$ cell class, based on *line geometry*, $D\mathcal{L}_\mathcal{K}$ loses its full rank only when the friction cone at the $S$ contact at $x_1$ is tangent to the line segment connecting the $I$ contacts at $x_2$ and $x_3$. However, in *tame* stances the friction cone at $x_1$ lies strictly above the plane spanned by the three contacts. The Jacobian $D\mathcal{L}_\mathcal{K}$ thus has full rank on both cell classes, which are therefore mapped into the interior of $\mathcal{W}$. Similar arguments hold for the remaining cell classes except $SI$, $II$, $SSI$, $SSS$, $SSSS$, and $SSSSS$.

## 4.3 The Critical Contact Forces at a K-Contact Stance

The following proposition characterizes the *critical contact forces* which satisfy the condition $\mathsf{rank}(\mathsf{D}\mathcal{L}_\mathcal{K}) = 5$ in the cell classes listed above in Theorem 2. The image of these critical contact forces under $\mathcal{L}$ will form the boundary of the net wrench cone $\mathcal{W}$ in $\mathcal{B}$'s wrench space.

**Proposition 4.2** (**Critical Contact Forces**). *For each cell class listed in Theorem 2, the* **critical contact forces** *which are possibly mapped to the boundary of the net wrench cone $\mathcal{W}$ satisfy the conditions:*

**1. Cell classes SI and II:** *The entire cells consist of critical contact forces.*

**2. Cell class *SSI*:** *The cells of this class are parametrized by $(\lambda_1, \phi_1)$, $(\lambda_2, \phi_2)$, and $f_3 \in \mathbb{R}^3$. The critical contact forces satisfy the two scalar equations:*

$$\begin{aligned} \boldsymbol{\eta}_1(\phi_1) \cdot (x_1 - x_3) &= 0 \\ \boldsymbol{\eta}_2(\phi_2) \cdot (x_2 - x_3) &= 0 \end{aligned} \tag{12}$$

*where $\boldsymbol{\eta}_i(\phi_i)$ is the normal to the friction cone's tangent plane $\Delta_i(\phi_i)$ for $i = 1, 2$.*

**3. Cell class *SSS*:** *The cells of this class are parametrized by $(\lambda_i, \phi_i)$ for $i = 1, 2, 3$. The critical contact forces are described by force angles $(\phi_1, \phi_2, \phi_3)$ satisfying the equation:*

$$\det \begin{bmatrix} \bar{\boldsymbol{s}} \cdot \boldsymbol{\nu}_1(\phi_1) & \bar{\boldsymbol{s}} \cdot \boldsymbol{\nu}_2(\phi_2) & \bar{\boldsymbol{s}} \cdot \boldsymbol{\nu}_3(\phi_3) \\ \bar{\boldsymbol{t}} \cdot \boldsymbol{\nu}_1(\phi_1) & \bar{\boldsymbol{t}} \cdot \boldsymbol{\nu}_2(\phi_2) & \bar{\boldsymbol{t}} \cdot \boldsymbol{\nu}_3(\phi_3) \\ \bar{\boldsymbol{n}} \cdot (x_1 \times \boldsymbol{\nu}_1(\phi_1)) & \bar{\boldsymbol{n}} \cdot (x_2 \times \boldsymbol{\nu}_2(\phi_2)) & \bar{\boldsymbol{n}} \cdot (x_3 \times \boldsymbol{\nu}_3(\phi_3)) \end{bmatrix} = 0 \tag{13}$$

*where* $\boldsymbol{\nu}_i(\phi_i) = \bar{\boldsymbol{n}} \times \boldsymbol{\eta}_i(\phi_i)$, $\bar{\boldsymbol{n}}$ *is a unit normal to the plane spanned by* $x_1, x_2, x_3$ *and* $(\bar{\boldsymbol{s}}, \bar{\boldsymbol{t}})$ *are orthonormal tangent vectors to that plane.*

**4. Cell class *SSSS*:** *The cells of this class are parametrized by* $(\lambda_i, \phi_i)$ *for* $i = 1, 2, 3, 4$. *The critical contact forces are described by angles* $(\phi_1, \phi_2, \phi_3, \phi_4)$ *satisfying three equations:*

$$\det \begin{bmatrix} \bar{\boldsymbol{s}}_i \cdot \boldsymbol{\nu}_i(\phi_i) & \bar{\boldsymbol{s}}_i \cdot \boldsymbol{\nu}_{i+1}(\phi_{i+1}) & \bar{\boldsymbol{s}}_i \cdot \boldsymbol{\nu}_{i+2}(\phi_{i+2}) \\ \bar{\boldsymbol{t}}_i \cdot \boldsymbol{\nu}_i(\phi_i) & \bar{\boldsymbol{t}}_i \cdot \boldsymbol{\nu}_{i+1}(\phi_{i+1}) & \bar{\boldsymbol{t}}_i \cdot \boldsymbol{\nu}_{i+2}(\phi_{i+2}) \\ \bar{\boldsymbol{n}}_i \cdot (x_i \times \boldsymbol{\nu}_i(\phi_i)) & \bar{\boldsymbol{n}}_i \cdot (x_{i+1} \times \boldsymbol{\nu}_{i+1}(\phi_{i+1})) & \bar{\boldsymbol{n}}_i \cdot (x_{i+2} \times \boldsymbol{\nu}_{i+2}(\phi_{i+2})) \end{bmatrix} = 0 \qquad i = 1, 2, 3 \tag{14}$$

*where index addition is modulo four. In these equations* $\boldsymbol{\nu}_i(\phi_i) = \bar{\boldsymbol{n}}_i \times \boldsymbol{\eta}_i(\phi_i)$, *where* $\bar{\boldsymbol{n}}_i$ *is a unit normal to the plane spanned by the contacts* $x_i$, $x_{i+1}$, $x_{i+2}$ *and* $(\bar{\boldsymbol{s}}_i, \bar{\boldsymbol{t}}_i)$ *are orthonormal tangent vectors to that plane.*

**5. Cell class *SSSSS*:** *The cells of this class are parametrized by* $(\lambda_i, \phi_i)$ *for* $i = 1 \ldots 5$. *The critical contact forces are described by angles* $(\phi_1, \phi_2, \phi_3, \phi_4, \phi_5)$ *satisfying five equations:*

$$\det \begin{bmatrix} \bar{\boldsymbol{s}}_i \cdot \boldsymbol{\nu}_i(\phi_i) & \bar{\boldsymbol{s}}_i \cdot \boldsymbol{\nu}_{i+1}(\phi_{i+1}) & \bar{\boldsymbol{s}}_i \cdot \boldsymbol{\nu}_{i+2}(\phi_{i+2}) \\ \bar{\boldsymbol{t}}_i \cdot \boldsymbol{\nu}_i(\phi_i) & \bar{\boldsymbol{t}}_i \cdot \boldsymbol{\nu}_{i+1}(\phi_{i+1}) & \bar{\boldsymbol{t}}_i \cdot \boldsymbol{\nu}_{i+2}(\phi_{i+2}) \\ \bar{\boldsymbol{n}}_i \cdot (x_i \times \boldsymbol{\nu}_i(\phi_i)) & \bar{\boldsymbol{n}}_i \cdot (x_{i+1} \times \boldsymbol{\nu}_{i+1}(\phi_{i+1})) & \bar{\boldsymbol{n}}_i \cdot (x_{i+2} \times \boldsymbol{\nu}_{i+2}(\phi_{i+2})) \end{bmatrix} = 0 \qquad i = 1 \ldots 5 \tag{15}$$

*where index addition is modulo five. In these equations* $\boldsymbol{\nu}_i(\phi_i) = \bar{\boldsymbol{n}}_i \times \boldsymbol{\eta}_i(\phi_i)$, *where* $\bar{\boldsymbol{n}}_i$ *is a unit normal to the plane spanned by the contacts* $x_i$, $x_{i+1}$, $x_{i+2}$ *and* $(\bar{\boldsymbol{s}}_i, \bar{\boldsymbol{t}}_i)$ *are orthonormal tangent vectors to that plane.*

The detailed proof of Proposition 4.2 appears in the supplementary document. Geometric interpretation of the criticality conditions in equations (12)-(15), as well as explanations of their dimensionality, are given as follows. In the cell class $SSI$, condition (12) implies that the forces $f_1 \in S_1$ and $f_2 \in S_2$ are directed such that the tangent planes $\Delta_1(\phi_1)$ and $\Delta_2(\phi_2)$ to the friction cones $C_1$,$C_2$ are both passing through the contact $x_3$. This condition is illustrated in the three-contact stance of Figure 3(a). Criticality can be viewed by the fact that infinitesimal changes in $f_1$ and $f_2$ within the friction cone tangent planes, accompanied by infinitesimal changes in $f_3 \in I_3$, will generate zero net torque about the intersection line of the two tangent planes $\Delta_1(\phi_1)$, $\Delta_2(\phi_2)$, which passes trough $x_3$. Thus, the image of the critical contact forces under $\mathcal{L}$ lies in a five-dimensional linear subspace in $\mathcal{B}$'s wrench space of net wrenches. Condition (12) gives a finite number of solution pairs, $(\phi_1^*, \phi_2^*)$, which are held fixed while the magnitudes $\lambda_1, \lambda_2 > 0$ and the three components of $f_3$ vary freely within the $SSI$ cell, thus spanning a five-dimensional sub-manifold of the cell.

In the cell class $SSS$, condition (13) implies that the three forces $f_1, f_2, f_3$ are directed such that the intersection point $z$ of the friction cone tangent planes $\Delta_1(\phi_1)$,$\Delta_2(\phi_2)$,$\Delta_3(\phi_3)$ lies on the plane spanned by $x_1$, $x_2$, and $x_3$. As an example, this condition is illustrated in the three-contact stance of Figure 3(b). Criticality of these contact forces can be explained as follows. Small changes in $f_i$ along its friction cone tangent plane can be partitioned into changes along the vector $z - x_i$, and changes along the orthogonal complement $(z - x_i) \times \boldsymbol{\eta}_i$, where $\boldsymbol{\eta}_i$ is the tangent plane's normal. The changes in $f_1$,$f_2$,$f_3$ along the $z - x_i$ components only span a two-dimensional subspace of net wrenches, $V_1$, since they generate forces in the plane spanned by the contacts $x_1, x_2, x_3$, while contributing zero torque about a line normal to that plane which passes through $z$. The changes in $f_1$,$f_2$,$f_3$ along the complementary components generate a three-dimensional subspace, $V_2$, of net wrenches. Thus, infinitesimal changes in contact force within the cell SSS only generate a five-dimensional subspace, $V_1 + V_2$, of net wrenches in $\mathbb{R}^6$. Condition (13) implies that the angles $(\phi_1, \phi_2, \phi_3)$ lie in a two dimensional solution set of (13), while the magnitudes $\lambda_1, \lambda_2, \lambda_3 > 0$ vary freely within the $SSS$ cell. Thus, the critical forces form a five-dimensional sub-manifold of the cell.

In the cell classes $SSSS$ and $SSSSS$, conditions (14) or (15) imply that each possible triplet of forces $f_i \in S_i$ must simultaneously satisfy the same 3-contact criticality relation as in (13). Condition (14) gives a system of three equations, so that the angles $(\phi_1, \phi_2, \phi_3, \phi_4)$ lie in a one-dimensional solution set, while the magnitudes $\lambda_1, \lambda_2, \lambda_3, \lambda_4 > 0$ vary freely within the cell. Thus, critical forces form a five-dimensional sub-manifold within $SSSS$. In the cell class $SSSSS$, condition (15) gives a system of five equations, yielding a finite number of solutions for the angles $(\phi_1, \ldots, \phi_5)$. These angles are held fixed while the magnitudes $\lambda_1, \ldots, \lambda_5 > 0$ vary freely within the cell, thus forming a five-dimensional liner subspace of $SSSSS$. Unlike the previous cases of three-contact cells $SSI$ and $SSS$, we cannot provide an intuitive description for the five-dimensional linear subspace of wrenches generated by critical forces from cells $SSSS$ and $SSSSS$.

Importantly, the conditions which define the critical contact forces in Proposition 4.2 are only *necessary* for finding points on the boundary of the net wrench cone $\mathcal{W}$. That is, critical contact forces in a cell $\mathcal{K}$ can be mapped under $\mathcal{L}$ to the *interior* rather than the boundary of $\mathcal{W}$. The next lemma specifies a sign condition that will be used to identify which critical contact forces are mapped to the actual boundary of $\mathcal{W}$.

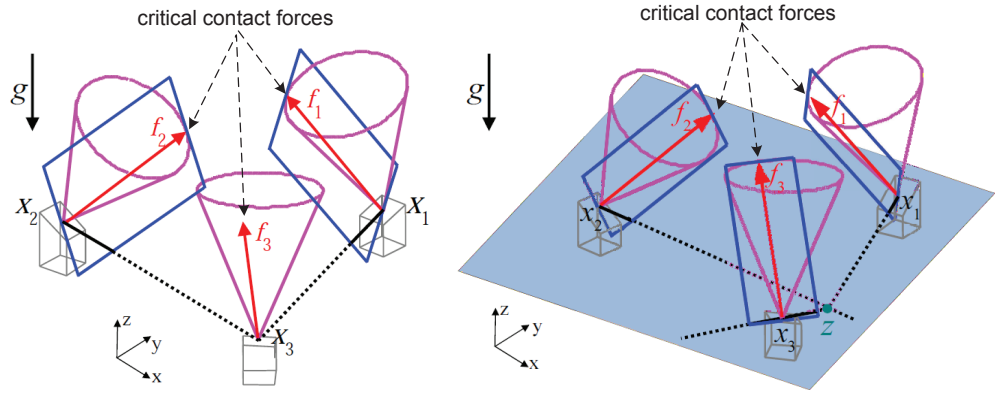


Figure 3: The critical contact forces in (a) an $SSI$ cell, and (b) an $SSS$ cell of a three-contact stance with $\mu = 0.4$ at the contacts. The contacts are $x_1 = (8, 0, 1)$, $x_2 = (4, 4\sqrt{3}, 1.2)$, $x_3 = (0, 0, 1)$, with contact normals $n_i = (\sin\alpha_i \sin\beta_i, -\cos\alpha_i \sin\beta_i, \cos\beta_i)$ such that $(\alpha_1, \beta_1) = (70°, -20°)$, $(\alpha_2, \beta_2) = (-15°, 34°)$, $(\alpha_3, \beta_3) = (-70°, -10°)$.

**Lemma 4.3.** *Let $\mathcal{K}$ be a cell of the set $C \subset \mathbb{R}^{3k}$, and let $\boldsymbol{f}^* = (f_1^*, \ldots, f_k^*)$ be critical contact forces in $\mathcal{K}$. The wrench $\boldsymbol{w}^* = \mathcal{L}(\boldsymbol{f}^*)$ lies on the boundary of the net wrench cone $\mathcal{W}$ if there exists a five-dimensional separating hyperplane, $H \subset \mathbb{R}^6$, passing through $\boldsymbol{w}^*$ such that all wrenches $\boldsymbol{w} \in \mathcal{W}$ lie on the* **same side** *of $H$ in $\mathbb{R}^6$. That is, there exists a sign $\sigma \in \{-1, +1\}$ satisfying the condition:*

$$\sigma(\boldsymbol{w} \cdot \boldsymbol{\eta}_H) \geq 0 \qquad \text{for all } \boldsymbol{w} \in \mathcal{W}, \tag{16}$$

*where $\boldsymbol{\eta}_H \in \mathbb{R}^6$ is the normal to the hyperplane $H$ in $\mathbb{R}^6$.*

A key observation is that the criticality conditions of Proposition 4.2 imply the existence of a five-dimensional hyperplane, $H$, which is *locally tangent* to the image of a cell $\mathcal{K}$ at a candidate boundary point $\boldsymbol{w}^* \in \mathcal{W}$, where the normal $\boldsymbol{\eta}_H$ is precisely the left kernel of the Jacobian $D\mathcal{L}_\mathcal{K}$ at $\boldsymbol{f}^*$. Thus, one has to check that the $\mathcal{L}$-images of all cells other than $\mathcal{K}$ satisfy condition (16). This leads to the following proposition which formulates the separation conditions for the cell classes listed in Theorem 2.

**Proposition 4.4 ($\mathcal{W}$ Boundary Condition).** *For each cell class listed in Theorem 2, the critical contact forces whose image under $\mathcal{L}$ lies on the actual boundary of the net wrench cone $\mathcal{W}$ satisfy the sign conditions:*
**1. Cell classes SI and II:** *The entire cells consist of critical contact forces. Their image under $\mathcal{L}$ lies on the boundary of $\mathcal{W}$ if and only if there exists a sign $\sigma \in \{-1, +1\}$ satisfying the inequalities:*

$$\sigma\left((x_2 - x_1) \cdot (x_i - x_1) \times n_i\right) \geq 0 \qquad i = 3 \ldots k \tag{17}$$

*where $n_i$ is the terrain's unit normal at $x_i$.*
**2. Cell class SSI:** *The critical contact forces are associated with fixed angles, $(\phi_1^*, \phi_2^*)$, determined by (12). Their image under $\mathcal{L}$ lies on the boundary of $\mathcal{W}$ if and only if there exists a sign $\sigma \in \{-1, +1\}$ satisfying the inequalities:*

$$\begin{aligned} &\sigma(\boldsymbol{\nu}^* \cdot (x_i - x_3) \times n_i \geq 0 && i{=}1{,}2 \\ &\sigma\left(\boldsymbol{\nu}^* \cdot (x_i - x_3) \times \boldsymbol{u}_i(\phi_i)\right) \geq 0 && \text{for all } \phi_i \in \mathbb{R},\ i = 4 \ldots k \end{aligned} \tag{18}$$

*where $\boldsymbol{\nu}^* = \boldsymbol{\eta}_1(\phi_1^*) \times \boldsymbol{\eta}_2(\phi_2^*)$ is collinear with the intersection line of the tangent planes $\Delta(\phi_1^*)$ and $\Delta(\phi_2^*)$.*
**3. Cell classes SSS, SSSS, SSSSS:** *The critical contact forces are associated with angles $\phi_i$ satisfying condition (13), (14), or (15). Let $z \in \Delta$ denote the intersection point of the friction cone tangent planes $\Delta_1(\phi_1)$, $\Delta_2(\phi_2)$, $\Delta_3(\phi_3)$, where $\Delta$ is the plane spanned by $x_1$, $x_2$, and $x_3$. The image of the critical contact forces under $\mathcal{L}$ lies on the boundary of $\mathcal{W}$ if and only if there exists a sign $\sigma \in \{-1, +1\}$ satisfying the inequalities:*

$$\begin{aligned} &\sigma\big(\bar{\boldsymbol{n}} \cdot ((x_i - z) \times \boldsymbol{\eta}_i(\phi_i))\big) \geq 0 && i = 1, 2, 3 \\ &\sigma\big(\bar{\boldsymbol{n}} \cdot \boldsymbol{u}_i(\phi_i) + \bar{\boldsymbol{\tau}} \cdot ((x_i - z) \times \boldsymbol{u}_i(\phi_i))\big) \geq 0 && \phi_i \in \mathbb{R} \text{ for } i = 4 \ldots k \end{aligned} \tag{19}$$

*where $\bar{\boldsymbol{n}}$ is the unit normal to $\Delta$, $\boldsymbol{n}_i(\phi_i)$ is the normal to the tangent plane $\Delta(\phi_i)$ for $i = 1, 2, 3$, and $\bar{\boldsymbol{\tau}}(\phi_1, \phi_2, \phi_3) = [\boldsymbol{\eta}_1(\phi_1)\, \boldsymbol{\eta}_2(\phi_2)\, \boldsymbol{\eta}_3(\phi_3)]^{-1} \boldsymbol{c}$ such that $\boldsymbol{c} = (c_1, c_2, c_3)$ are the direction cosines of the tangent planes $\Delta_1(\phi_1), \Delta_2(\phi_2), \Delta_3(\phi_3)$ with respect to $\Delta$.*

The proof of Proposition 4.4 appears in the supplementary document. Note that conditions (18) and (19) require checking the sign of expressions $\bar{\boldsymbol{n}} \cdot \boldsymbol{u}_i(\phi_i) + \bar{\boldsymbol{\tau}} \cdot (x_i \times \boldsymbol{u}_i(\phi_i))$ and $\bar{\boldsymbol{n}} \cdot \boldsymbol{u}_i(\phi_i) + \bar{\boldsymbol{\tau}} \cdot ((x_i - z) \times \boldsymbol{u}_i(\phi_i))$ for $i = 4 \ldots k$ such that $\phi_i$ varies freely in $\mathbb{R}$. These tests can be reduced to computing extremum values of a function of the form $g(\phi_i) = a_i + b_i \cos\phi_i + c_i \sin\phi_i$, which can be computed in closed form.

# 5 The Boundary of the Feasible Equilibrium Region

The boundary of the feasible equilibrium region $\widetilde{\mathcal{R}}$ is now obtained, based on the scheme outlined in Section 3. Next, computation of $\widetilde{\mathcal{R}}$ for stances with $k>5$ contacts by using simpler computations of 4-tuples or 5-tuples of contacts is described. Finally, the section discusses the non-static motion modes that can develop at the contacts when $\mathcal{B}$'s center of mass crosses the boundary of the feasible equilibrium region. The results in this section are stated for tame stances only. For non-tame stances, while the same characterization of types of boundary curves holds, the region $\widetilde{\mathcal{R}}$ is not guaranteed to be bounded, see discussion in section 8.

## 5.1 The Boundary Curves of $\widetilde{\mathcal{R}}$

To compute the boundary of $\widetilde{\mathcal{R}}$, recall from Section 3 that the intersection of the net wrench cone boundary, $\mathsf{bdy}(\mathcal{W})$, with the affine plane of gravitational wrenches, $L$, represents the two sides of the equilibrium stance equation (2). This equation can be decomposed into three sets of equations:

$$\begin{array}{ll} (i) & f_1+\cdots+f_k=\boldsymbol{e} \\ (ii). & \boldsymbol{e}\cdot(x_1\times f_1+\cdots+x_k\times f_k)=0 \\ (iii) & \mathbf{E}(x_1\times f_1+\cdots+x_k\times f_k)=\mathbf{E}(\boldsymbol{x}_c\times\boldsymbol{e}) \qquad \mathbf{E}=\left(\begin{array}{ccc}1&0&0\\0&1&0\end{array}\right) \end{array} \tag{20}$$

where the forces are scaled such that $\|f_g\|=1$, $\boldsymbol{e}$ is the upward vertical direction in $\mathbb{R}^3$, and $\mathbf{E}$ projects vectors in $\mathbb{R}^3$ onto $\mathbb{R}^2$. Parts (i) and (ii) of (20) form a system of four equations. Thus, critical contact forces lying on a five-dimensional sub-manifold of a cell $\mathcal{K}$ which also satisfy parts (i) and (ii), form a one-dimensional curve whose image under $\mathcal{L}$ lies on the intersection $\mathsf{bdy}(\mathcal{W})\cap L$. These forces are linearly related to the horizontal position of $\mathcal{B}$'s center of mass $\tilde{\boldsymbol{x}}_c$ via part (iii) of (20). This relation can then be inverted in order to obtain the linear map to boundary pieces of $\widetilde{\mathcal{R}}$:

$$\tilde{\boldsymbol{x}}_c=-\mathbf{E}\big(\boldsymbol{e}\times(x_1\times f_1+\cdots+x_k\times f_k)\big). \tag{21}$$

The following main theorem characterizes the boundary curves of $\widetilde{\mathcal{R}}$ associated with the cell classes listed in Theorem 2. The boundary curves of $\widetilde{\mathcal{R}}$ are formulated for a specific contact indices assignment where the $S_i$ contacts receive the lowest indices, then the $I_i$ contacts, and last the $O_i$ contacts, but represents all possible index permutations.

**Theorem 3 (Boundary of $\widetilde{\mathcal{R}}$).** *The horizontal cross-section of the feasible equilibrium region of a tame $k$-contact stance, $\widetilde{\mathcal{R}}\subset\mathbb{R}^2$, is bounded by a closed loop consisting of up to* **five types** *of curves:*

*1.* **SI/II segment:** *Associated with non-zero contact forces $(f_1,f_2)$ and $f_i{=}\vec{0}$ for $i=3\ldots k$. This* **linear segment** *lies on the support polygon edge connecting the projected contacts $\tilde{x}_1$ and $\tilde{x}_2$ in $\mathbb{R}^2$.*

*2.* **SSI segment:** *Associated with non-zero contact forces $(f_1,f_2,f_3){\in}S_1{\times}S_2{\times}I_3$ and $f_i{=}\vec{0}$ for $i=4\ldots k$. The forces $(f_1,f_2)$ are parametrized by $f_i=\lambda_i\boldsymbol{u}_i(\phi_i^*)$, where $(\phi_1^*,\phi_2^*)$ are discrete solutions of (12) that also satisfy the separation condition (18). Each solution $(\phi_1^*,\phi_2^*)$ determines a* **linear segment** *that lies on the horizontal projection of the intersection line of the friction cone tangent planes $\Delta_1(\phi_1^*)$ and $\Delta_2(\phi_2^*)$.*

*3.* **SSS curve:** *Associated with non-zero contact forces $(f_1,f_2,f_3){\in}S_1{\times}S_2{\times}S_3$ and $f_i{=}\vec{0}$ for $i=4\ldots k$. The forces $(f_1,f_2,f_3)$ are parametrized by $f_i=\lambda_i\boldsymbol{u}(\phi_i)$, such that $(\phi_1,\phi_2,\phi_3)$ satisfy the scalar equation (13) combined with the scalar equation associated with parts (i) and (ii) of (20):*

$$\det\left[\begin{array}{ccc}\mathbf{E}\boldsymbol{u}_1(\phi_1) & \mathbf{E}\boldsymbol{u}_2(\phi_2) & \mathbf{E}\boldsymbol{u}_3(\phi_3)\\ \boldsymbol{e}\cdot(x_1{\times}\boldsymbol{u}_1(\phi_1)) & \boldsymbol{e}\cdot(x_2{\times}\boldsymbol{u}_2(\phi_2)) & \boldsymbol{e}\cdot(x_3{\times}\boldsymbol{u}_3(\phi_3))\end{array}\right]=0. \tag{22}$$

*The angles $(\phi_1,\phi_2,\phi_3)$ satisfying (13) and (22) as well as the separation condition (19) form a one-dimensional solution set which is mapped by (21) to a* **convex arc** *on the boundary of $\widetilde{\mathcal{R}}$.*

*4.* **SSSS curve:** *Associated with non-zero contact forces $(f_1,f_2,f_3,f_4){\in}S_1{\times}S_2{\times}S_3{\times}S_4$ and $f_i{=}\vec{0}$ for $i=5\ldots k$. The forces $(f_1,f_2,f_3,f_4)$ are parametrized by $f_i=\lambda_i\boldsymbol{u}(\phi_i)$, such that $(\phi_1,\phi_2,\phi_3,\phi_4)$ satisfy (14) as well as the separation condition (19). The contact forces that satisfy (14) combined with parts (i) and (ii) of (20) form a one-dimensional solution set which is mapped by (21) to a* **convex arc** *on the boundary of $\widetilde{\mathcal{R}}$.*

*5.* **SSSSS segment:** *Associated with non-zero contact forces $(f_1,\ldots,f_5){\in}S_1{\times}\ldots{\times}S_5$ and $f_i{=}\vec{0}$ for $i=6\ldots k$. The forces $(f_1,\ldots,f_5)$ are parametrized by $f_i=\lambda_i\boldsymbol{u}(\phi_i^*)$, such that $(\phi_1^*,\ldots,\phi_5^*)$ are discrete solutions of (15) that also satisfy the separation condition (19). The contact forces that satisfy (15) combined with parts (i) and (ii) of (20) are mapped by (21) to a* **linear segment** *on the boundary of $\widetilde{\mathcal{R}}$.*

The proof of the Theorem 3 appears in the supplementary document. The theorem thus establishes that the boundary of $\widetilde{\mathcal{R}}$ consists of *three types* of linear segments and *two types* of convex arcs. Note that convexity of

the arcs associated with the $SSS$ and $SSSS$ cells follows directly from the fact that the feasible equilibrium regions always forms a convex region in $I\!R^2$.

Computation of the boundary curves of $\widetilde{\mathcal{R}}$ via the linear map (21) is next described in some detail. For $SI/II$ cell, the equilibrium equation (20) implies that the contact forces $f_1, f_2$ must lie within the horizontal plane $H_{12}$ passing through the contacts $x_1$ and $x_2$. The net wrench generated by the contact forces lies along an affine line, whose endpoints are determined by the frictional constraints $f_i \in C_i \cap H_{12}$ for $i = 1, 2$, which give linear inequalities. Thus, the corresponding boundary segments of $\widetilde{\mathcal{R}}$ can be obtained via linear programming as explained in (Or and Rimon, 2006). For $SSI$ cell, the directions of contact forces $f_1$ and $f_2$ are determined by (22), and the equilibrium equation (20) implies that the contact force $f_3$ must lie within the horizontal plane $H$ that contains the intersection line $\Delta_1(\phi_1^*) \cap \Delta_2(\phi_2^*)$. The net wrench generated by the contact forces lies along an affine line, whose endpoints are determined by the frictional constraints $\lambda_1, \lambda_2 \geq 0$ and $f_3 \in C_3 \cap H$, which give linear inequalities. Thus, the corresponding boundary segments of $\widetilde{\mathcal{R}}$ can also be obtained via linear programming. To compute the $SSS$ boundary curves, for each solution $(\phi_1, \phi_2, \phi_3)$ of (13) and (22) that satisfies the inequalities in (19), the force magnitudes $\lambda_1, \lambda_2, \lambda_3$ are obtained by solving the $3 \times 3$ linear system imposed by part (i) of (20):

$$\lambda_1 \boldsymbol{u}_1(\phi_1) + \lambda_2 \boldsymbol{u}_2(\phi_2) + \lambda_3 \boldsymbol{u}_3(\phi_3) = \boldsymbol{e}$$

Every solution satisfying $\lambda_1, \lambda_2, \lambda_3 \geq 0$ is then mapped by (21) to a point $\tilde{\boldsymbol{x}}_c$ on the boundary of $\widetilde{\mathcal{R}}$. To compute the $SSSS$ boundary curves, for each value of $(\phi_1, \phi_2, \phi_3, \phi_4)$ on the solution curve of the system (14) that also satisfies the inequalities (19), the force magnitudes $\lambda_1, \lambda_2, \lambda_3, \lambda_4$ are obtained by solving the $4 \times 4$ linear system imposed by parts (i) and (ii) of (20):

$$\begin{aligned} &\lambda_1 \boldsymbol{u}_1(\phi_1) + \lambda_2 \boldsymbol{u}_2(\phi_2) + \lambda_3 \boldsymbol{u}_3(\phi_3) + \lambda_4 \boldsymbol{u}_4(\phi_4) = \boldsymbol{e} \\ &\boldsymbol{e} \cdot \big(\lambda_1 x_1 \times \boldsymbol{u}_1(\phi_1) + \lambda_2 x_2 \times \boldsymbol{u}_2(\phi_2) + \lambda_3 x_3 \times \boldsymbol{u}_3(\phi_3) + \lambda_4 x_4 \times \boldsymbol{u}_4(\phi_4)\big) = 0. \end{aligned}$$

Every solution satisfying $\lambda_1, \ldots, \lambda_4 \geq 0$ is then mapped by (21) to a point $\tilde{\boldsymbol{x}}_c$ on the boundary of $\widetilde{\mathcal{R}}$. Finally, the boundary segments associated with $SSSSS$ cell are obtained as follows. The direction of forces $\phi_1 \ldots \phi_5$ are discrete solutions of (15) that also satisfy the separation condition (19). The equilibrium equation (20) then gives a linear system of 6 equations in 7 scalar unknowns, which are $(\tilde{\boldsymbol{x}}_c, \lambda_1 \ldots \lambda_5)$. The solution set is an affine line whose endpoints are determined by the linear inequalities $\lambda_1 \ldots \lambda_5 \geq 0$. Thus, the endpoints of the boundary segment of $\tilde{\boldsymbol{x}}_c$ can be obtained via linear programming. Further explanation on numerical computation of $\widetilde{\mathcal{R}}$ boundary curves appear in (Or and Rimon, 2014), while code implementation of MATLAB functions are included in the supplementary material.

## 5.2 Practical computation of the Feasible Equilibrium Region for $K \geq 5$ Contacts

While Theorem 3 describes the boundary of the feasible equilibrium region of tame stances for arbitrary number of contacts, stances with $k \geq 5$ contacts can practically be treated by considering the feasible equilibrium regions associated with all possible four-tuples or five-tuples of contacts. The following proposition describes two equivalent ways for computing the feasible equilibrium region of such stances.

**Proposition 5.1.** *In a tame $k$-contact stance supported by $k > 5$ frictional contacts, the feasible equilibrium region $\widetilde{\mathcal{R}}$ can be obtained by computing the feasible equilibrium region of each* **five-tuple** *of the $k$ contacts, $\widetilde{\mathcal{R}}_{j_1 j_2 j_3 j_4 j_5}$, then taking the* **convex hull** *of these regions:*

$$\widetilde{\mathcal{R}} = \mathsf{conv}\Big\{\widetilde{\mathcal{R}}_{j_1 j_2 j_3 j_4 j_5} : 1 \leq j_1, j_2, j_3, j_4, j_5 \leq k\Big\}.$$

*Equivalently, for $k \geq 5$ contacts, $\widetilde{\mathcal{R}}$ can be obtained by computing the feasible equilibrium region of each* **four-tuple** *of the $k$ contacts, $\widetilde{\mathcal{R}}_{j_1 j_2 j_3 j_4}$, then taking the* **convex hull** *of these regions: $\widetilde{\mathcal{R}} = \mathsf{conv}\{\widetilde{\mathcal{R}}_{j_1 j_2 j_3 j_4} : 1 \leq j_1, j_2, j_3, j_4 \leq k\}$.*

**Proof sketch:** The boundary of $\widetilde{\mathcal{R}}$ consists of up to five types of curves, each associated with a specific combination of two, three, four, or five critical contact forces according to Theorem 3. Since $\widetilde{\mathcal{R}}$ forms a convex set in $I\!R^2$, it must be the *convex hull* of the feasible equilibrium regions associated with all five-tuple of the $k$ contacts. Next consider the four-tuples formulation. An $SSSSS$ boundary curve of $\widetilde{\mathcal{R}}$ forms a bounded *linear segment* in $I\!R^2$. An endpoint of this segment occurs at a center of mass location where the magnitude of one of the five critical contact forces associated with the $SSSSS$ cell reduces to zero. Each endpoint is therefore an endpoint of an adjacent $SSSS$ boundary curve of $\widetilde{\mathcal{R}}$. By convexity of $\widetilde{\mathcal{R}}$, the $SSSSS$ segments can be obtained by connecting the endpoints of the $SSSS$ arcs by straight line segments. This operation is equivalent to taking the convex hull of the feasible equilibrium regions associated with all four-tuples of the $k$ contacts. □

Based on Proposition 5.1, the feasible equilibrium region of a five-contact stance can be computed as the convex hull of its four-contact equilibrium regions associated with the given set of contacts, as illustrated in the numerical example of Figure 7(a).

### 5.3 Onset of Non-Static Motion Modes at the Contacts

Consider the situation where the body $\mathcal{B}$ is supported in static equilibrium by a tame contact arrangement. Let the body's center of mass *slowly* move such that its horizontal projection, $\tilde{\boldsymbol{x}}_c$, crosses the boundary of the feasible equilibrium region. At this instant static equilibrium can no longer be maintained and non-static motion will develop at the contacts. These imminent motion modes depend on the type of boundary curve of $\widetilde{\mathcal{R}}$ being crossed by $\mathcal{B}$'s center of mass. Thus, consider a boundary curve of $\widetilde{\mathcal{R}}$ associated with critical contact forces in a particular cell $\mathcal{K}$ of the product set $C_1 \times \cdots \times C_k$. The contact forces $(f_1, \ldots, f_k) \in \mathcal{K}$ are associated with $n_S$ choices of $S_i$ components, $n_I$ choices of $I_i$ components, and $k - n_S - n_I$ choices of $O_i$ components. An $S_i$ component represents contact force on the friction cone boundary, an $I_i$ component represents contact force in the friction cone interior, and an $O_i$ component represents zero contact force. Hence, the non-static modes that will develop at the contacts depend on the $O_i$, $S_i$, and $I_i$ components of the cell $\mathcal{K}$. When $\mathcal{K}$ contains an $O_i$ component, the body will *break contact* at $x_i$ and the contact force $f_i$ will vanish as a result of this contact separation. When $\mathcal{K}$ contains an $S_i$ component, the body will start *slipping* at $x_i$ and the contact force $f_i$ will remain on the friction cone boundary for some finite time interval. When $\mathcal{K}$ contains an $I_i$ component, the body will start *rolling* at $x_i$ and the contact force $f_i$ will remain in the i'th friction cone interior for some finite time interval.

Based on this insight, the crossing of the feasible equilibrium region boundary curves can thus be associated with the following non-static motion modes. First consider the case where the body's center of mass crosses an $SI/II$ boundary segment of $\widetilde{\mathcal{R}}$. In this case one expects that the body will start rolling about the line connecting the two $I$ contacts, or start slipping at the $S$ contact and rolling at the $I$ contact, such that all other contacts separate during either motion. While either of these motions can develop at the contacts, intuition suggests that an $II$ rolling motion will usually develop at the contacts. When the body's center of mass crosses an $SSI$ boundary segment of $\widetilde{\mathcal{R}}$, one expects the onset of rolling about the $I$ contact accompanied by slippage at the two $S$ contacts, while all other contacts separate during this motion. Finally, when the body's center of mass crosses an $SSS$, $SSSS$, or $SSSSS$ boundary curve of $\widetilde{\mathcal{R}}$, one expects the onset of slippage at the three, four, or five $S$ contacts while all other contacts separate during this motion. Some of these non-static motion modes are further discussed in Section 7.

## 6 Computational Examples of the Feasible Equilibrium Region

This section describes three computational examples of the feasible equilibrium region for tame stances supported by frictional contacts. The three examples match three experiments to be discussed in Section 7, and will be used to compare the theory against actual measurements. All supporting contacts are assumed to have a coefficient of friction $\mu = 0.155$ which corresponds to the experiments. The contact locations will be specified in cylindrical coordinates as $x_i = (r\cos\gamma_i, r\sin\gamma_i, z_i) \in I\!R^3$ for $i = 1 \ldots k$, where $\gamma_i$ is the angle between the projected contact point, $\tilde{x}_i$, and the $x$-axis in $I\!R^2$. All contacts are thus located on a vertical cylinder of radius $r$ centered at the origin. Length parameters such as the radius $r$ will be specified using arbitrary length units. The terrain's outward unit normal at each contact point, $n_i$, will be expressed by its $x$-axis and $z$-axis rotation angles as $n_i = (\sin\alpha_i \sin\beta_i, -\cos\alpha_i \sin\beta_i, \cos\beta_i)$ for $i = 1 \ldots k$. In particular, $\alpha_i = \beta_i = 0$ indicates a vertically aligned contact normal, $n_i = \boldsymbol{e}$.

**Three-contact stance:** Consider the three-contact stance depicted in Figure 4(a). The contacts are located at $x_1 = (r\cos\gamma_1, r\sin\gamma_1, 1.0)$, $x_2 = (r\cos\gamma_2, r\sin\gamma_2, 1.0)$, and $x_3 = (r\cos\gamma_3, r\sin\gamma_3, 1.0 + r/4)$; such that $\gamma_1 = 150°$, $\gamma_2 = 30°$, $\gamma_3 = 90°$, and $r = 8/\sqrt{3}$. The contact normal angles are given by $(\alpha_1, \beta_1) = (0, 0)$, $(\alpha_2, \beta_2) = (0, 0)$, and $(\alpha_3, \beta_3) = (20°, 15°)$. This stance can be verified to be *tame,* so that $\widetilde{\mathcal{R}} \subseteq \mathcal{P}$ for this stance. However, $x_3$ is not quasi-flat since its friction cone, $C_3$, does not contain the upward vertical direction $\boldsymbol{e}$. Since $\tilde{x}_3$ forms a vertex of the support polygon $\mathcal{P}$ which lies *outside* $\widetilde{\mathcal{R}}$, the feasible equilibrium region forms a strict subset of the support polygon in this example.

Figure 4(b) plots the feasible equilibrium region of the three-contact stance in the $(x, y)$ plane. Note that $\widetilde{\mathcal{R}}$ forms a convex region within the support polygon $\mathcal{P}$, bounded by two $II$ segments, one $SSI$ segment, and one $SSS$ arc. The $II$ segments are associated with critical contact forces from the cells $I_1 \times I_2 \times O_3$ and $O_1 \times I_2 \times I_3$. Both segments lie on the support polygon edges, as noted in the discussion that followed Theorem 3. The $SSI$ segment is associated with critical contact forces from the cell $I_1 \times S_2 \times S_3$. This

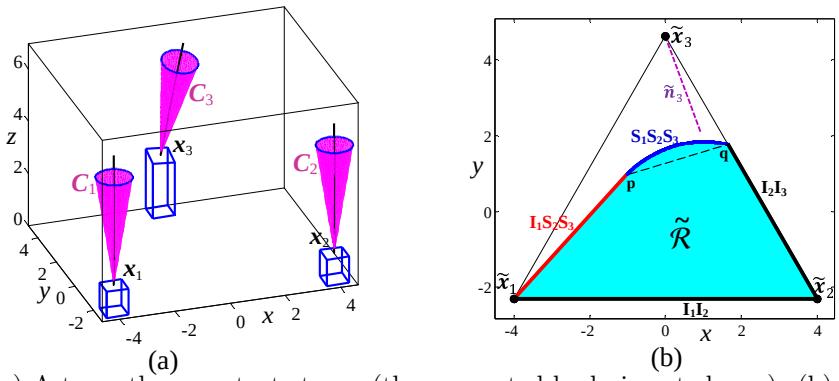


Figure 4: (a) A tame three-contact stance (the supported body is not shown). (b) Top view of the feasible equilibrium region $\widetilde{\mathcal{R}}$ and its three types of boundary curves.

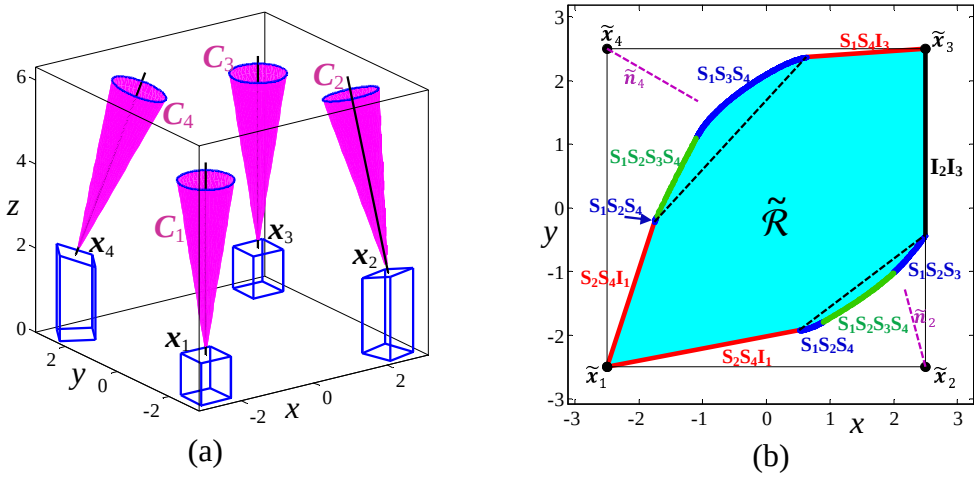


Figure 5: (a) A tame four-contact stance (the supported body is not shown). (b) Top view of the feasible equilibrium region $\widetilde{\mathcal{R}}$ and its four types of boundary curves.

segment lies on the horizontal projection of the intersection line of the tangent planes to the friction cones $C_2$ and $C_3$, as stated in the discussion that followed Theorem 3, . The $SSS$ arc is associated with critical contact forces from the cell $S_1 \times S_2 \times S_3$. While the computation of this arc involves solution of nonlinear equations specified in Theorem 3, the linear $II$ and $SSI$ boundary segments are easily computed by solving simple linear programs (Or and Rimon, 2014). Thus, a reasonable approximation for $\widetilde{\mathcal{R}}$ would be to replace the $SSS$ arc by a linear segment connecting its endpoints $p$ and $q$, as shown with dashed line in Figure 4(b). This gives a conservative polygonal region which is contained in $\widetilde{\mathcal{R}}$ and captures 97% of its total area.

**Four-contact stance:** Next consider the four-contact stance depicted in Figure 5(a). The contacts are located at $x_1 = (r\cos\gamma_1, r\sin\gamma_1, 1.0)$, $x_2 = (r\cos\gamma_2, r\sin\gamma_2, 1.0 + r/4)$, $x_3 = (r\cos\gamma_3, r\sin\gamma_3, 1.0)$, and $x_4 = (r\cos\gamma_4, r\sin\gamma_4, 1.0 + r/4)$; such that $\gamma_1 = 135°$, $\gamma_2 = 45°$, $\gamma_3 = 45°$, $\gamma_4 = 135°$, and $r = 5/\sqrt{2}$. The contact normal angles are given by $(\alpha_1, \beta_1) = (0, 0)$, $(\alpha_2, \beta_2) = (15°, -15°)$, $(\alpha_3, \beta_3) = (0, 0)$, and $(\alpha_4, \beta_4) = (60°, 20°)$. This stance can be verified to be *tame*, so that $\widetilde{\mathcal{R}} \subseteq \mathcal{P}$ for this stance. However, the contacts $x_2$ and $x_4$ are not quasi-flat as their friction cones, $C_2$ and $C_4$, do not contain the vertical upward direction $\boldsymbol{e}$. Since the projected contacts $\tilde{x}_2$ and $\tilde{x}_4$ are vertices of the support polygon $\mathcal{P}$, they must lie outside $\widetilde{\mathcal{R}}$. One therefore expects that here, too, $\widetilde{\mathcal{R}}$ will be a strict subset of the support polygon $\mathcal{P}$. Figure 5(b) plots the feasible equilibrium region $\widetilde{\mathcal{R}}$ for this stance in the $(x, y)$ plane. It forms a convex region bounded by one $II$ segment, three $SSI$ segments, four $SSS$ arcs, and two $SSSS$ arcs. The labels near each boundary curve indicate which critical contact forces generated this curve. For instance, the $I_2I_3$ segment on the right side of $\widetilde{\mathcal{R}}$ is generated by critical contact forces in the cell $O_1 \times I_2 \times I_3 \times O_4$, while the $S_2S_4I_1$ segment on the bottom of $\widetilde{\mathcal{R}}$ is generated by critical contact forces in the cell $I_1 \times S_2 \times O_3 \times S_4$. Note the appearance of two $S_1S_2S_3S_4$ boundary arcs, which most likely belong to a single closed loop embedded in $\widetilde{\mathcal{R}}$. Using only the $II$ and $SSI$ line segments and connecting their endpoints by straight lines as shown with dashed segments in Figure 5(b), one obtains a conservative polygonal approximation of $\widetilde{\mathcal{R}}$ which reasonably captures 92% of its total area.

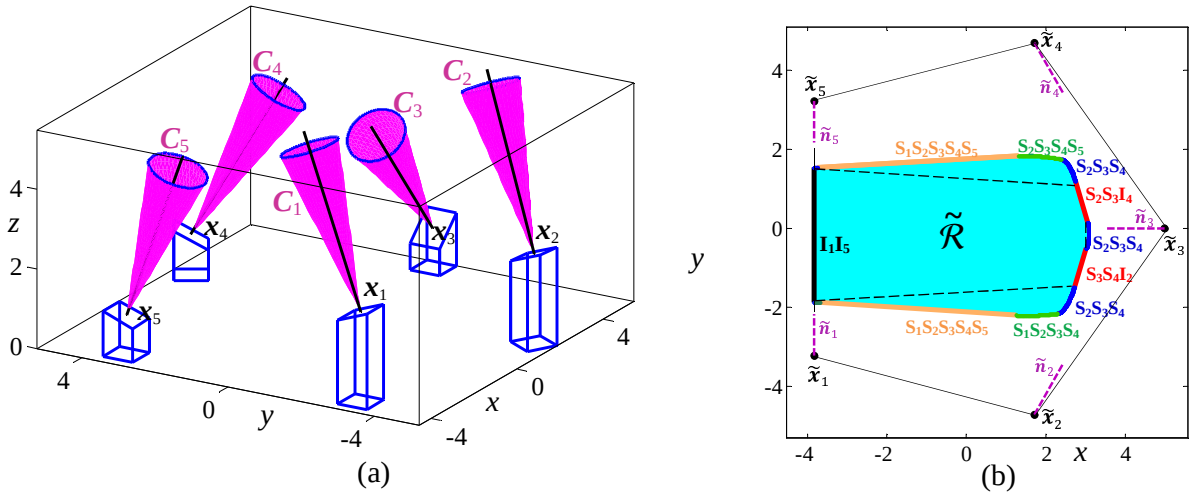


Figure 6: (a) A tame five-contact stance (the supported body is not shown). (b) Top view of the feasible equilibrium region $\widetilde{\mathcal{R}}$ and its five types of boundary curves.

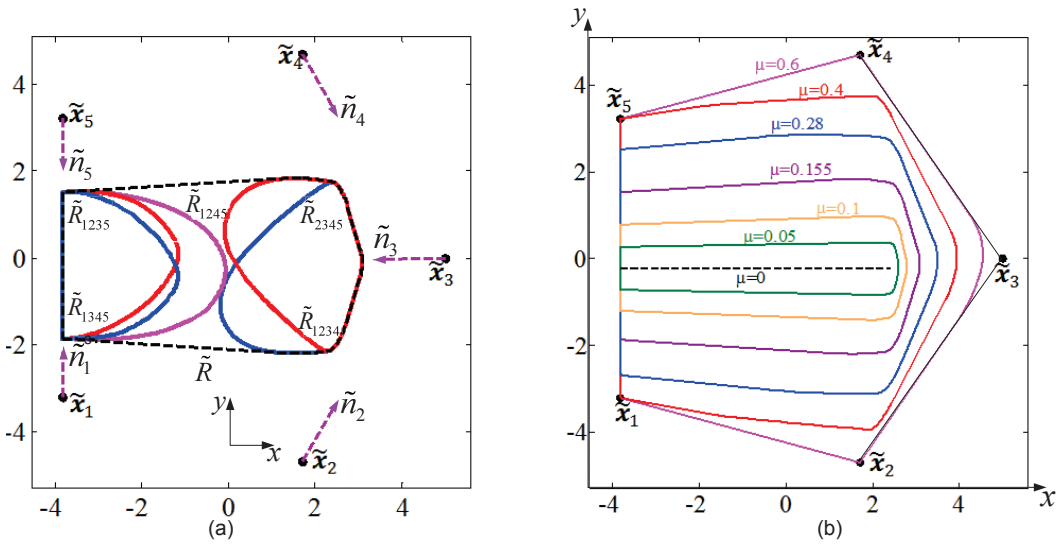


Figure 7: (a) The feasible equilibrium regions of all contact quadruples of the five-contact stance. (b) The feasible equilibrium region plotted as a function of $\mu$.

**Five-contact stance:** Last consider the five-contact stance depicted in Figure 6(a). The contacts are located at $x_1 = (r\cos\gamma_1, r\sin\gamma_1, 1.0 + r/4)$, $x_2 = (r\cos\gamma_2, r\sin\gamma_2, 1.0 + r/4)$, $x_3 = (r\cos\gamma_3, r\sin\gamma_3, 1.0)$, $x_4 = (r\cos\gamma_4, r\sin\gamma_4, 1.0)$, and $x_5 = (r\cos\gamma_5, r\sin\gamma_5, 1.0)$; such that $\gamma_1 = -140°$, $\gamma_2 = -70°$, $\gamma_3 = 0$, $\gamma_4 = 70°$, $\gamma_5 = 140°$, and $r = 5.0$. The contact normal angles are given by $(\alpha_1, \beta_1) = (0, -20°)$, $(\alpha_2, \beta_2) = (-30°, -30°)$, $(\alpha_3, \beta_3) = (90°, -40°)$, $(\alpha_4, \beta_4) = (30°, 30°)$, and $(\alpha_5, \beta_5) = (20°, 20°)$. This five-contact stance can be verified to be *tame*, so that $\widetilde{\mathcal{R}} \subseteq \mathcal{P}$ for this stance. Since all five contacts are non quasi-flat at this stance, the projected contacts which form the vertices of the support polygon $\mathcal{P}$ lie *outside* $\widetilde{\mathcal{R}}$. Hence, the stance's feasible equilibrium region $\widetilde{\mathcal{R}}$ lies *strictly inside* the support polygon $\mathcal{P}$, as can be seen in Figure 6(b). The boundary of $\widetilde{\mathcal{R}}$ consists of one $II$ segment, two $SSI$ segments, five $SSS$ arcs, four $SSSS$ arcs, and two $SSSSS$ segments. In particular, there are *very short* $SSS$ and $SSSS$ arcs on each side of the $II$ segment, which are hardly visible in Figure 6(b). Using only the $II$ and $SSI$ line segments and connecting their endpoints by straight lines as shown with dashed segments in Figure 6(b), one obtains a conservative polygonal approximation of $\widetilde{\mathcal{R}}$ which captures 81% of its total area.

The five-contact stance of Figure 6(a) is next used to verify the convex hull property stated in Proposition 5.1. According to this proposition, the feasible equilibrium region of the five-contact stance can be obtained by taking the *convex hull* of all four-contact feasible equilibrium regions. Figure 7(a) shows the feasible equilibrium regions associated with all contact quadruples. The convex hull of these regions gives the

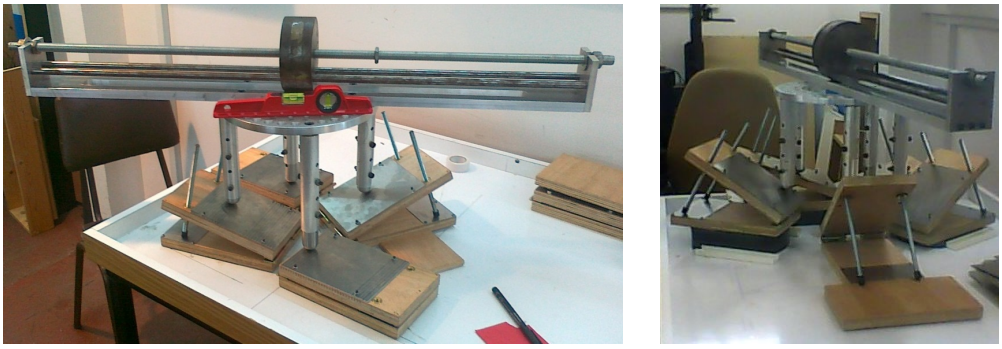

(a) (b)

Figure 8: Two experimental setups of a legged mechanism with a movable center of mass.

feasible equilibrium region $\widetilde{\mathcal{R}}$ of the five-contact stance (indicated with dashed curve). Finally, Figure 7(b) depicts the dependency of $\widetilde{\mathcal{R}}$ on the coefficient of friction $\mu$. Starting with a high value of $\mu = 0.85$, all contacts are quasi-flat and the stance is tame. Hence $\widetilde{\mathcal{R}} = \mathcal{P}$ for this value of $\mu$. For $\mu = 0.6$, the contact $x_3$ is no longer quasi-flat and $\tilde{x}_3$ no longer lies in $\widetilde{\mathcal{R}}$. For $\mu = 0.4$, the contacts $x_2$, $x_3$ and $x_4$ are no longer quasi-flat and consequently $\tilde{x}_2$, $\tilde{x}_3$ and $\tilde{x}_4$ no longer lie in $\widetilde{\mathcal{R}}$. For $\mu = 0.28$, all five contacts cease to be quasi-flat, but the boundary of $\widetilde{\mathcal{R}}$ still contains one $II$ segment that lies on a support polygon edge connecting $\tilde{x}_1$ with $\tilde{x}_5$. The region $\widetilde{\mathcal{R}}$ is next plotted for $\mu = 0.155$ (which corresponds to Figure 6(b)), then for $\mu = 0.1$ and $\mu = 0.05$. Eventually $\mu = 0$ and the contacts become frictionless. The region $\widetilde{\mathcal{R}}$ associated with such contacts shrinks to a single line segment, shown with dashed line at the center of Figure 7(b).

# 7 Experimental Results

This section describes experiments that measure the feasible equilibrium region of a legged mechanism prototype having a movable center of mass, which is supported on a frictional terrain against gravity. The objective of these experiments is to validate the analytical characterization of the feasible equilibrium region $\widetilde{\mathcal{R}}$ of tame stances supported by multiple frictional contacts. As shown in Figure 8, the legged mechanism consists of a rigid central ring made of aluminum, extendible legs made of steel, and a movable heavy steel cylinder that determines the mechanism's center of mass location. The central ring has a diameter of 240 mm and is drilled with 36 holes that allow attachment of three, four, or five legs. Each leg can be assembled in three different lengths of 30 mm, 60 mm, and 90 mm. Each leg ends with a spherical footpad made of steel, which maintains a frictional point contact with the supporting terrain. The supporting terrain consists of stainless steel plates whose slope angles can be adjusted with a lead screw mounted against a horizontal support plate (Figure 8). The heavy steel cylinder which determines the mechanism's center of mass slides on a linear guide mounted on top of the central ring (Figure 8). The linear guide can be attached at 15° orientation increments using screws that can be inserted in 24 holes drilled into the central ring. The mass of each extendible leg is 0.82 kg, the central ring and linear guide combined mass is 6.17 kg, and the movable cylinder mass is 4.25 kg.

As a preliminary stage, the coefficient of static friction between the footpads and supporting plates, $\mu$, was experimentally measured. A horizontal force was applied to the legged mechanism while its footpads were supported by horizontal plates. The horizontal force was applied by hanging a variable weight on a string attached to the mechanism through a pulley. By measuring the critical weight that caused slippage at the footpads, the *average* coefficient of friction, $\bar{\mu}$, has been determined to be $\bar{\mu} = 0.155$ with standard deviation of $\sigma = \pm 0.02$.

Each experiment started by assembling the mechanism with the chosen number of legs, with the desired leg lengths and relative positions of these legs. The mechanism was then placed in *static equilibrium* on the supporting plates, whose position and slopes was set according to the chosen stance arrangement. The movable heavy cylinder was initially placed above the central ring's center, then it was *slowly* shifted outward along its linear guide in 1 mm increments. After each 1 mm increment, the contacts were checked in order to verify that the mechanism maintained its static equilibrium. This process continued until the mechanism's center of mass reached the boundary of the feasible equilibrium region, where a critical event of contact breakage or slippage was observed at one or more of the supporting contacts. The critical center of mass position and the observed non-static motion mode were recorded, and the process was iterated 10 times in order to collect multiple measurements. Next, the center of mass linear guide was mounted at a different orientation with respect to the ring, and the entire measurement process was repeated for the new linear

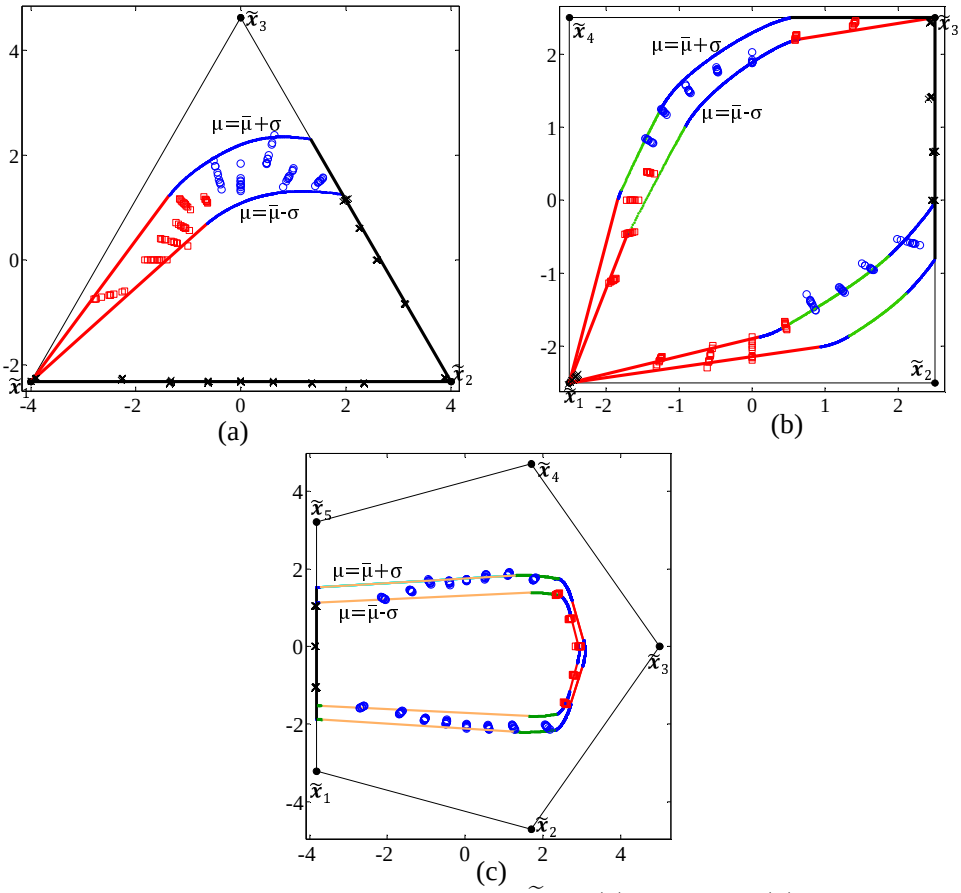


Figure 9: Experimental results of measured boundary of $\widetilde{\mathcal{R}}$ for (a) three legs, (b) four legs, and (c) five legs.

guide orientation. The measured orientations eventually covered a full circle with 15° resolution, giving a discrete mapping of the boundary of $\widetilde{\mathcal{R}}$.

The experiments were conducted for three, four, and five-legged stances. These stances are identical to the computational examples shown in Figures 4, 5, and 6, where the length units in these figures are scaled by a common factor in order to match $r$ with the radius of the central ring. Measurements of the critical center of mass locations on the boundary of the feasible equilibrium region for the three, four, and five-legged stances are shown in Figures 9(a),(b),(c) respectively. The theoretically computed inner and outer equilibrium regions overlayed with solid curves correspond to friction coefficients $\mu = \bar{\mu} \pm \sigma$. Three different non-static motion modes were visually detected in the experiments: circled points mark rolling over two supporting contacts while all other contacts are separating, squared points mark rolling about one supporting contact while the other contacts are either slipping or separating, x points mark simultaneous slippage at three or more supporting contacts while all other contacts are separating. A more elaborate distinction between the non-static contact modes involving slippage at three or more contacts turned out to be too challenging under the current experimental setup.

In the experimental measurements, 90% of the measured boundary points fall between boundaries computed for $\mu = \bar{\mu} \pm \sigma$, while *all* points fall within the range of two standard deviations. The experimental measurements thus show good agreement with the theoretical computation of the feasible equilibrium region $\widetilde{\mathcal{R}}$ in all three stances. In particular, it can be seen that the $II$ boundary points associated with two-contact rolling are very accurate and display *very small* variations of up to 2 mm. On the other hand, measurement of boundary points that involve slippage suffer from *much larger* variations on the order of 10-15 mm. The reason for the difference in the variances is as follows. The $II$ boundary points are associated with onset of rolling about two contacts while all other contacts are separating. The location of these boundary points depends only on the supporting contact positions, which were measured with relatively high accuracy. In contrast, the location of boundary points associated with onset of slippage depends on the stance's geometric data as well as on the precise value of the coefficient of friction $\mu$ at the contacts. The value of $\mu$ has been determined experimentally and is known to be a sensitive quantity subject to large deviations. These deviations explain the high measurement variance of boundary points associated with slippage at three or

more supporting contacts. Nevertheless, most of these boundary points fall well within the range between the computed boundaries for $\bar{\mu} \pm \sigma$, thus validating the analytic characterization of the feasible equilibrium region.

# 8 Conclusion

The paper characterized the feasible equilibrium region of tame stances supported by multiple frictional contacts against gravity. These stances represent the statically stable postures of a legged mechanism supported by the same set of contacts. The feasible equilibrium region of a given stance, $\widetilde{\mathcal{R}}$, is a subset of the support polygon. In particular when the friction cones at the supporting contacts do not contain the vertical upward direction $\boldsymbol{e}$, the region $\widetilde{\mathcal{R}}$ forms a *strict subset* of the support polygon $\mathcal{P}$. On such uneven stances the support polygon $\mathcal{P}$ *can no longer be safely used* to choose statically stable equilibrium postures for the legged mechanism. The analytical and experimental results reported in this paper are therefore essential for safe legged locomotion over uneven terrains. The results extend to more general terrains as discussed below.

The paper established that the feasible equilibrium region of a tame $k$-contact stance, $\widetilde{\mathcal{R}} \subset I\!R^2$, forms a convex set bounded by up to *five types* of boundary curves. The first type are $SI/II$ linear segments. The crossing of these segments is associated with onset of rolling motion about two supporting contacts while all other contacts are separating. The second type are $SSI$ linear segments. The crossing of these segments is associated with onset of slippage at two contacts, rolling at a third contact, and separation at all other contacts. The third and fourth types are nonlinear $SSS$ and $SSSS$ boundary curves. The crossing of these curves is associated with onset of simultaneous slippage at three or four contacts while all other contacts are separating. The fifth type are $SSSSS$ linear segments, whose crossing is associated with onset of simultaneous slippage at five contacts while all other contacts are separating. Importantly, the feasible equilibrium region associated with higher numbers of contacts is bounded by the same five types of boundary curves, and can be obtained by taking the convex hull of the individual 4- or 5-contact equilibrium regions.

Future extensions of the results include the following topics. The most important extension is the need to develop efficient methods to compute the feasible equilibrium region for a series of $k$-contact stances during legged locomotion. While the linear boundary segments of $\widetilde{\mathcal{R}}$ can be efficiently computed as low-dimensional linear programs, efficient computation of the nonlinear boundary curves is a challenging problem. These nonlinear curves can be approximated by replacing the exact friction cones with multi-facet polyhedra, as done in (Or and Rimon, 2014; Caron et al., 2015). This approach is also implemented in the computational code that we provided in the supplementary material (**?**). Another promising direction would be to merge the paper's analytical results with the iterative projection algorithms in Bretl's computational algorithm (Bretl and Lall, 2008; Prete et al., 2016), which iteratively compute outer and inner polygonal approximations of $\widetilde{\mathcal{R}}$. Another possible extension concerns *non-tame* stances, which are typical to vertical climbing scenarios. When a legged mechanism climbs over steep terrains and acquires a non-tame stance, the feasible equilibrium region associated with the given set of contacts is no longer bounded within the support polygon, and may even lie entirely *outside* the support polygon (see example in (Bretl and Lall, 2008)). Although the five types of boundary curves of $\widetilde{\mathcal{R}}$ do not change on non-tame stances, a problem may arise when $\widetilde{\mathcal{R}}$ becomes *unbounded* in some directions. In particular, the five-tuples convex hull closure property (Proposition 5.1) may not hold once $\widetilde{\mathcal{R}}$ becomes unbounded. A systematic method for identifying which non-tame stances result in unbounded $\widetilde{\mathcal{R}}$ as well as its computation are still open problems.

A longer term issue concerns synthesis and experimental validation of quasistatic legged locomotion planners based on feasible equilibrium regions (Geva and Shapiro, 2012; Hauser et al., 2008; Caron et al., 2015; Prete et al., 2016). While it is tempting to demonstrate the utility of such planners, equilibrium feasibility must be carefully augmented with the following additional considerations. The first consideration concerns the ambiguous rigid-body dynamics incurred by the presence of friction at the contacts (Lotstedt, 1981; Mason and Wang, 1988; Rajan et al., 1987). One must ensure that a feasible equilibrium is dynamically non-ambiguous, or a *strong equilibrium* (Lynch and Mason, 1996; Pang and Trinkle, 2000). A second issue concerns the *stability* of a candidate equilibrium posture, which consists of resistance to disturbance wrenches generated by moving parts of the mechanism (Or and Rimon, 2006), as well as stability with respect to perturbations of the legged mechanism's equilibrium state. The latter stability must account for the *hybrid dynamics* induced by non-smooth transitions associated with contact slippage, contact breakage and impacts at recovering contacts, which are still open problems in the area of hybrid dynamical systems (Leine and van de Wouw, 2008; Várkonyi and Or, 2016).

# References


J. E. Bares and D. S. Wettergreen. DANTE II: technical description, results, and lessons learned. *Int. J. of Robotics Research*, 18(7):621–649, 1999.

S. Blind, C. McCullough, S. Akella, and J. Ponce. Manipulating parts with an array of pins: A method and a machine. *The Int. J. of Robotics Research*, 20(10):808–818, 2001.

J.-D. Boissonnat, O. Devillers, and S. Lazard. Motion planning of legged robots. *SIAM Journal of Computing*, 30(1):218–246, 2000.

T. Bretl and S. Lall. A fast and adaptive test of static equilibrium for legged robots. In *IEEE Int. Conf. on Robotics and Automation*, pages 1109 – 1116, 2006.

T. Bretl and S. Lall. Testing static equilibrium for legged robots. *IEEE Transactions on Robotics*, 24(4): 794–807, 2008.

S. Caron, Q.-C. Pham, and Y. Nakamura. Leveraging cone double description for multi-contact stability of humanoids with applications to statics and dynamics. *Robotics: Science and System*, 2015.

A. Dandurand. The rigidity of compound spatial grid. *Structural Topology*, 10:41–56, 1984.

J. Duffy. *Statics and Kinematics with Applications to Robotics*. Cambridge University Press, 1996.

M. A. Erdmann. An exploration of nonprehensile two-palm manipulation. *The Int. J. of Robotics Research*, 17(5), 1998.

F. Fen, M. Shoham, and R. Longman. Lyapunov stability of force-controlled grasps with a multifingered hand. *Int. J. of Robotics Research*, 15(2):137–154, 1996.

Y. Geva and A. Shapiro. A combined potential function and graph search approach for free gait generation of quadruped robots. In *IEEE Int. Conf. on Robotics and Automation*, pages 5371–5376, 2012.

B. Goodwine and J. Burdick. Motion planning for kinematic stratified systems with application to quasi-static legged locomotion and finger gaiting. *IEEE Transactions on Automatic Control*, 18(2):209–222, 2002.

V. Guillemin and A. Pollack. *Differential Topology*. Prentice-Hall, Inc., New Jersey, 1974.

E. Guizzo and E. Ackerman. *DARPA Robotics Challenge: Here Are the Official Details*. http://spectrum.ieee.org/automaton/robotics/humanoids, 2012.

L. Han, J. Trinkle, and Z. Li. Grasp analysis as linear matrix inequality problems. *IEEE Trans. on Robotics and Automation*, 16(6):663–674, 2000.

K. Hauser, T. Bretl, J.-C. Latombe, K. Harada, and B. Wilcox. Motion planning for legged robots on varied terrain. *The International Journal of Robotics Research*, 27(11-12):1325–1349, 2008.

K. Hirai, M. Hirose, Y. Haikawa, and T. Takenaka. The development of honda humanoid robot. In *IEEE Int. Conf. on Robotics and Automation*, pages 1321–1326, 1998.

M. Hirose, Y. Haikawa, T. Takenaka, and K. Hirai. Development of humanoid robot ASIMO. In *Int. Conf. on Intelligent Robots and Systems (IROS)*, pages 310–320, 2001.

D. W. Hong and R. J. Cipra. Optimal contact force distribution for multi-limbed robots. *Journal of Mechanical Design*, 128(3):566–573, 2006.

K. Kaneko, F. Kanehiro, M. Morisawa, K. Akachi, G. Miyamori, A. Hayashi, and N. Kanehira. Humanoid robot HRP-4 - humanoid robotics platform with lightweight and slim body. In *Int. Conf. on Intelligent Robots and Systems (IROS)*, pages 4400–4407, 2011.

E. Krotkov and R. Simmons. Perception, planning, and control for autonomous walking with the ambler planetary rover. *Int. J. of Robotics Research*, 15(2):155–180, 1996.

J. Kuffner, K. Nishiwaki, S. Kagami, M. Inaba, and H. Inoue. Motion planning for humanoid robots under obstacle and dynamic balance constraints. In *IEEE Int. Conf. on Robotics and Automation*, pages 692–698, 2001.

R. I. Leine and N. van de Wouw. Stability properties of equilibrium sets of nonlinear mechanical systems with dry friction and impact. *Nonlinear Dynamics*, 51:551–583, 2008.

G. F. Liu, J. Li, and Z. X. Li. Coordinated manipulation of objects by multifingered robotic hand in contact space and active joint space. In *IEEE Int. Conf. on Robotics and Automation*, pages 3743–3748, 2002.

V. G. Loc, I. M. Koo, D. T. Tran, S. Park, H. Moon, and H. R. Choi. Body workspace of quadruped walking robot and its applicability in legged locomotion. *J. of Intelligent and Robotic Systems*, 67(3-4):271–284, 2012.

P. Lotstedt. Coulomb friction in two-dimensional rigid body systems. *Zeitschrift fur Angewandte Mathematik und Mechanik*, 61:605–615, 1981.

K. M. Lynch and M. T. Mason. Stable pushing: Mechanics, controllability, and planning. *The Int. J. of Robotics Research*, 15(6):533–556, 1996.

A. Madhani and S. Dubowsky. Motion planning of mobile multi-limb robotic systems subject to force and friction constraints. In *IEEE Int. Conf. on Robotics and Automation*, pages 233–239, 1992.

D. W. Marhefka and D. E. Orin. Gait planning for energy efficiency in walking machines. In *IEEE Int. Conf. on Robotics and Automation*, pages 474–480, 1997.

M. T. Mason and J. K. Salisbury. *Robots Hands and the Mechanics of Manipulation*. MIT Press, Cambridge, MA, 1985.

M. T. Mason and Y. Wang. On the inconsistency of rigid-body frictional planar mechanics. In *IEEE Int. Conf. on Robotics and Automation*, pages 524–528, 1988.

J. M. McCarthy. *Introduction to Theoretical Kinematics*. MIT Press, 1990.

R. B. McGhee and A. A. Frank. On the stability properties of quadruped creeping gaits. *Mathematical Biosciences*, 3, 1968.

R. B. McGhee and G. I. Iswandhi. Adaptive locomotion of a multilegged robot over rough terrain. *IEEE Trans. on Systems, Man and Cybernetics*, 9(4):176–182, 1979.

K. Mirza and D. E. Orin. General formulation for force distribution in power grasps. In *IEEE Int. Conf. on Robotics and Automation*, pages 880–887, 1994.

M. P. Murphy, A. Saunders, C. Moreira, A. A. Rizzi, and M. Raibert. The LittleDog robot. *The Int. J. of Robotics Research*, 30(2):145–149, 2011.

P. D. Neuhaus, J. E. Pratt, and M. J. Johnson. Comprehensive summary of the institute for human and machine cognition's experience with LittleDog. *The Int. J. of Robotics Research*, 30(2):216–235, 2011.

V.-D. Nguyen. Constructing force-closure grasps. *The Int. J. of Robotics Research*, 7(3):3–16, 1988.

T. Omata and K. Nagata. Rigid body analysis of the indeterminate grasp force in power grasps. *IEEE Trans. on Robotics and Automation*, 16(1):46–54, 2000.

Y. Or and E. Rimon. Computation and graphical characterization of robust multiple-contact postures in two-dimensional gravitational environments. *Int. Journal of Robotics Research*, 25(11):1071–1086, 2006.

Y. Or and E. Rimon. Analytic characterization of a class of three-contact frictional equilibrium postures in three-dimensional gravitational environments. *Int. Journal of Robotics Research*, 29:3–22, 2010.

Y. Or and E. Rimon. Computation of frictional multi-contact equilibrium stances and postures on 3D uneven tame terrains. Tech. report, Dept. of ME, Technion, www.technion.ac.il/ izi/publications, Dec. 2014.

J. S. Pang and J. C. Trinkle. Stability characterizations of fixtured rigid bodies with coulomb friction. In *IEEE Int. Conf. on Robotics and Automation*, pages 361–368, 2000.

J. Park and Y. Youm. General ZMP preview control for bipedal walking. In *IEEE Int. Conf. on Robotics and Automation*, pages 2682–2687, 2007.

J. Park, K. Harada, and M. Kaneko. Enveloping grasp feasibility inequality. In *IEEE Int. Conf. on Robotics and Automation*, pages 2210–2216, 2001.

J. Ponce, S. Sullivan, A. Sudsang, J.-D. Boissonnat, and J.-P. Merlet. On computing four-finger equilibrium and force-closure grasps of polyhedral objects. *The Int. J. of Robotics Research*, 16(1):11–35, 1997.

A. D. Prete, S. Tonneau, and N. Mansard. Fast algorithms to test robust static equilibrium for legged robots. In *IEEE Int. Conf. on Robotics and Automation*, pages 1601–1607, 2016.

V. T. Rajan, R. Burridge, and J. T. Schwartz. Dynamics of rigid body in frictional contact with rigid walls. In *IEEE Int. Conf. on Robotics and Automation*, pages 671–677, 1987.

J. R. Rebula, P. D. Neuhaus, B. V. Bonnlander, M. J. Johnson, and J. E. Pratt. A controller for the LittleDog quadruped walking on rough terrain. In *IEEE Int. Conf. on Robotics and Automation*, pages 1467–1473, 2007.

T. Schlegl, M. Buss, T. Omata, and G. Schmidt. Fast dextrous regrasping with optimal contact forces and contact sensor-based impedance control. In *IEEE Int. Conf. on Robotics and Automation*, pages 103–108, 2001.

L. Sentis, B. Fernandez, and M. Slovich. Prediction and planning methods of bipedal dynamic locomotion over very rough terrains. In *15th Int. Symposium on Robotics Research (ISRR)*, 2011.

H.-K. Shin and B. K. Kim. Energy-efficient gait planning and control for biped robots utilizing the allowable zmp region. *IEEE Trans. on Robotics*, 30(4):986–993, 2014.

N. Simaan and M. Shoham. Singularity analysis of a class of composite serial in-parallel robots. *IEEE Trans. on Robotics and Automation*, 7(3):301–311, 2001.

T. Sugihara and Y. Nakamura. Contact phase invariant control for humanoid robot based on variable impedant inverted pendulum model. In *IEEE Int. Conf. on Robotics and Automation*, pages 51–56, 2003.

T. Takubo, Y. Imada, K. Ohara, Y. Mae, and T. Arai. Rough terrain walking for bipedal robot by using ZMP criteria map. In *IEEE Int. Conf. on Robotics and Automation*, pages 788–793, 2009.

P. L. Várkonyi and Y. Or. Lyapunov stability of a rigid body with two frictional contacts. *arXiv*, abs/1603.09672, 2016. URL `http://arxiv.org/abs/1603.09672`.

M. Vukobratovic and B. Borovac. Zero moment point — thirty five years of its life. *Int. J. of Humanoid Robotics*, 1(1):157–173, 2004.

B. H. Wilcox, T. Litwin, J. Biesiadecki, J. Matthews, M. Heverly, J. Morrison, J. Townsend, N. Ahmed, A. Sirota, and B. Cooper. ATHLETE: A cargo handling and manipulation robot for the moon. *J. of Field Robotics*, 24(5):421–434, 2007.

J. J. Xu, G. F. Liu, and Z. X. Li. On quality functions for grasp synthesis and fixture planning. In *IEEE Int. Conf. on Robotics and Automation*, pages 333–338, 2004.

K. Yokoi, F. Kanehiro, K. Kaneko, S. Kajita, K. Fujiwara, and H. Hirukawa. Experimental study of humanoid robot HRP-1S. *The Int. J. of Robotics Research*, 23(4-5):351–362, 2004.

Y. Yokokohji, S. Nomoto, and T. Yoshikawa. Static evaluation of humanoid robot postures constrained to the surrounding environment through their limbs. In *IEEE Int. Conf. on Robotics and Automation*, pages 1856–1863, 2002.

# Supplementary document - Proofs and Technical Details

This document contains proofs of Proposition 2.2, Theorem 2, Proposition 4.2, Proposition 4.4 and Theorem 3.

**Proposition 2.2.** *The feasible equilibrium region of a tame k-contact stance, $\widetilde{\mathcal{R}}$, is* **fully contained** *in the support polygon, $\widetilde{\mathcal{R}} \subseteq \mathcal{P}$. The converse relationship, $\mathcal{P} \subseteq \widetilde{\mathcal{R}}$, always holds for quasi-flat stances.*
**Proof:** First consider the relation $\widetilde{\mathcal{R}} \subseteq \mathcal{P}$. We have to show that every center of mass position $\boldsymbol{x}_c$ which satisfies the equilibrium condition (2) lies in $\mathcal{P}$. Let $l_{ij}$ denote the spatial line passing through $x_i$ and $x_j$. Since $f_i$ and $f_j$ generate zero torque about $l_{ij}$, the torque-balance part of (2) implies that the net torque generated by $f_g$ and $f_p$ about $l_{ij}$ must vanish. Since the stance is tame, $f_p$ satisfies $f_p \cdot \boldsymbol{n}_{ijp} \geq 0$ for all $f_p \in C_p$. Hence torque balance about $l_{ij}$ can be shown to imply that $\boldsymbol{x}_c$ must lie within the halfspace of $\mathbb{R}^3$ bounded by the vertical plane passing through the spatial segment $(x_i, x_j)$, such that the halfspace contains the point $x_p$. Repeating this argument for every segment $(x_i, x_j)$ on the boundary of $\mathcal{P}$, one concludes that $\boldsymbol{x}_c$ must lie within the vertical prism spanned by the contacts, which implies that $\widetilde{\mathcal{R}} \subseteq \mathcal{P}$. At a quasi-flat stance, each contact point can individually balance the gravitational force acting on $\mathcal{B}$. The vertical lines passing through the contacts therefore lie in $\mathcal{R}$. Since $\mathcal{R}$ forms a convex set of vertical lines in $\mathbb{R}^3$, it contains the vertical prism spanned by the contacts, which implies that $\mathcal{P} \subseteq \widetilde{\mathcal{R}}$ for quasi-flat stances. □

The rest of the proofs rely on basic facts from *line geometry* (Duffy, 1996; McCarthy, 1990), which require some notation. Consider a line $l$ passing through a point $p \in \mathbb{R}^3$ along a unit direction $v \in \mathbb{R}^3$. The *Plücker coordinates* of $l$ are defined as the vector $(v, p \times v) \in \mathbb{R}^6$. Using Plücker coordinates, the equilibrium stance condition (2) can be interpreted as *linear dependency* of the gravitational force line on the contact force lines. Linear subspaces in Plücker coordinates represent well known line collections. We will need the following flat and solid pencils.

**Definition 8.** *A* **flat pencil** *is a two-dimensional linear subspace in $\mathbb{R}^6$ spanned by two lines $(v_1, p \times v_1)$ and $(v_2, p \times v_2)$ intersecting at $p$. A* **solid pencil** *is a three-dimensional linear subspace in $\mathbb{R}^6$ spanned by three lines $(v_1, p \times v_1)$, $(v_2, p \times v_2)$, and $(v_3, p \times v_3)$ intersecting at $p$.*

A flat pencil represents all lines passing through a point $p$, such that the lines are embedded in a plane spanned by $(v_1, v_2)$ in $\mathbb{R}^3$. A solid pencil represents all lines passing through $p$ along all spatial directions in $\mathbb{R}^3$. To see were these pencils appear, recall that each friction cone is partitioned into three subsets: $C_i = O_i \cup I_i \cup S_i$. A flat pencil appears in the Jacobian of a wrench generated by contact forces $f_i \in S_i$. In this case $f_i = \lambda_i \boldsymbol{u}_i(\phi_i)$, and the Jacobian of the wrench $\boldsymbol{w}_i = (f_i, x_i \times f_i)$ is the $6 \times 2$ matrix:

$$D\boldsymbol{w}_i(\lambda_i, \phi_i) = \begin{pmatrix} \boldsymbol{u}_i(\phi_i) & \lambda_i \boldsymbol{u}_i'(\phi_i) \\ x_i \times \boldsymbol{u}_i(\phi_i) & \lambda_i x_i \times \boldsymbol{u}_i'(\phi_i) \end{pmatrix}.$$

The pair $(\boldsymbol{u}_i(\phi_i), \boldsymbol{u}_i'(\phi_i))$ spans the tangent plane $\Delta(\phi_i)$ to the friction cone boundary $S_i$. Since $\lambda_i$ appears as multiplicative parameter, the columns of $D\boldsymbol{w}_i$ span a flat pencil based at $x_i$ whose lines are embedded in $\Delta(\phi_i)$. A solid pencil appears in the Jacobian of a wrench generated by contact forces $f_i \in I_i$. In this case $f_i$ is parametrized by its cartesian coordinates, $f_i \in \mathbb{R}^3$, and the Jacobian of $\boldsymbol{w}_i = (f_i, x_i \times f_i)$ is the $6 \times 3$ matrix:

$$D\boldsymbol{w}_i(f_i) = \begin{pmatrix} I \\ [x_i \times] \end{pmatrix},$$

where $I$ is a $3 \times 3$ identity matrix, and $[x_i \times]$ is the $3 \times 3$ matrix which acts as cross-product on vectors, $[x_i \times] v = x_i \times v$ for $v \in \mathbb{R}^3$ (this notation will be used throughout the document). The columns of $D\boldsymbol{w}_i$ thus span a *solid pencil* based at the contact point $x_i$. The next lemma provides useful facts concerning linear dependency of pencils (see, e.g., (Dandurand, 1984; Ponce et al., 1997; Simaan and Shoham, 2001)).

**Lemma .1 (Linearly Dependent Pencils).** *Let $p_1, p_2, p_3$ be three points which do not lie along a common line in $\mathbb{R}^3$. The following relations hold for pencils based at these points.*

1. *Three flat pencils based at $p_1$, $p_2$, and $p_3$ are linearly dependent iff they intersect at a common point located on the plane spanned by the three points.*[2]
2. *Two flat pencils based at $p_1$ and $p_2$ and a solid pencil based at $p_3$ are linearly dependent*

[2] Three flat pencils containing three parallel lines are considered to be intersecting at infinity.

*iff the two flat pencils pass through the point $p_3$.*

3. *A flat pencil based at $p_1$ and two solid pencils based at $p_2$ and $p_3$ are linearly dependent iff the flat pencil at $p_1$ coincides with the plane spanned by the three points.*

Note that Lemma .1 refers to linear dependency of vectors in $\mathbb{R}^6$ which represent the lines' Plücker coordinates. The following theorem lists the cell classes the can possibly contribute five-dimensional pieces to the boundary of the net wrench cone $\mathcal{W}$.

**Theorem 2.** *The cell classes in $C_1 \times \cdots \times C_k$ whose image under $\mathcal{L}$ possibly contributes* **five-dimensional boundary pieces** *to the net wrench cone $\mathcal{W}$ at a generic tame k-contact stance are SI, II, SSI, SSS, SSSS, and SSSSS.*

**Proof:** Any five-dimensional cell in $C$ is generically mapped by $\mathcal{L}$ to a five-dimensional set which can contribute to the boundary of $\mathcal{W}$. Thus consider the cells in $C$ having dimension six or higher. When $D\mathcal{L}_\mathcal{K}$ has *full rank* on a cell $\mathcal{K}$ of dimension six or higher, the cell is mapped into the interior of $\mathcal{W}$ according to the inverse function theorem. The proof will therefore establish that $D\mathcal{L}_\mathcal{K}$ has full rank on each cell class *not* listed in the theorem.

**I. Cell classes associated with three non-zero contact forces.** We have to show that $D\mathcal{L}_\mathcal{K}$ has *full rank* on the cell classes $SII$ and $III$. First consider the $III$ cell class. The contact forces in a cell $\mathcal{K}$ of this class are parametrized by $(f_1, f_2, f_3) \in \mathbb{R}^9$. Using these parameters, the Jacobian of $\mathcal{L}_\mathcal{K} : \mathbb{R}^9 \to \mathbb{R}^6$ is the $6 \times 9$ matrix:

$$D\mathcal{L}_\mathcal{K} = \begin{pmatrix} I & I & I \\ [x_1\times] & [x_2\times] & [x_3\times] \end{pmatrix} \cong \begin{pmatrix} O & O & I \\ [(x_1-x_3)\times] & [(x_2-x_3)\times] & [x_3\times] \end{pmatrix},$$

where $I$ and $O$ are the identity and zero $3 \times 3$ matrices. The Jacobian has a non-trivial left kernel only when $x_2 - x_1$ and $x_3 - x_1$ are collinear vectors, which occurs only when the contacts lie on a common line in $\mathbb{R}^3$. Hence $D\mathcal{L}_\mathcal{K}$ has full rank on $III$ cells associated with generic stances.

Next consider the $SII$ cell class. Up to contact re-ordering a cell $\mathcal{K}$ has the form $\mathcal{K} = S_1 \times I_2 \times I_3$. The contact force $f_1 \in S_1$ is parametrized by $(\lambda_1, \phi_1)$, while the contact forces $(f_2, f_3) \in I_2 \times I_3$ are parametrized by $\mathbb{R}^6$. Using these parameters, the Jacobian of $\mathcal{L}_\mathcal{K} : \mathbb{R}^8 \to \mathbb{R}^6$ is the $6 \times 8$ matrix:

$$D\mathcal{L}_\mathcal{K} = \begin{pmatrix} \boldsymbol{u}_1(\phi_1) & \lambda_1\boldsymbol{u}_1'(\phi_1) & I & I \\ x_1\times\boldsymbol{u}_1(\phi_1) & \lambda_1 x_1\times\boldsymbol{u}_1'(\phi_1) & [x_2\times] & [x_3\times] \end{pmatrix}.$$

The two columns of $D\mathcal{L}_\mathcal{K}$ associated with $x_1$ span a *flat pencil* tangent to $S_1$, while the six columns associated with $x_2$ and $x_3$ span two *solid pencils* based at these points. Let $\Delta$ be the plane spanned by $x_1$, $x_2$, and $x_3$. Based on Lemma .1, one flat pencil at $x_1$ and two solid pencils at $x_2$ and $x_3$ are linearly dependent as vectors in $\mathbb{R}^6$ only when the flat pencil at $x_1$ coincides with the plane $\Delta$. It follows that $D\mathcal{L}_\mathcal{K}$ looses its full rank only when the friction cone at $x_1$ is *tangent* to $\Delta$. However, in *tame* stances the friction cone at $x_1$ lies strictly above $\Delta$. Hence $D\mathcal{L}_\mathcal{K}$ has full rank on the $SII$ cell class.

**II. Cell classes associated with four non-zero contact forces.** We have to show that $D\mathcal{L}_\mathcal{K}$ has *full rank* on the cell classes $SSSI$, $SSII$, $SIII$, and $IIII$. In the $SIII$ and $IIII$ cell classes, $D\mathcal{L}_\mathcal{K}$ has full rank in the generic case where the $I$ contacts do not lie on a common line in $\mathbb{R}^3$. In the $SSII$ cell class, up to contact re-ordering a cell $\mathcal{K}$ has the form $\mathcal{K} = S_1 \times S_2 \times I_3 \times I_4$. The Jacobian $D\mathcal{L}_\mathcal{K}$ is the $6 \times 10$ matrix:

$$D\mathcal{L}_\mathcal{K} = \begin{pmatrix} \boldsymbol{u}_1(\phi_1) & \lambda_1\boldsymbol{u}_1'(\phi_1) & \boldsymbol{u}_2(\phi_2) & \lambda_2\boldsymbol{u}_2'(\phi_2) & I & I \\ x_1\times\boldsymbol{u}_1(\phi_1) & \lambda_1 x_1\times\boldsymbol{u}_1'(\phi_1) & x_2\times\boldsymbol{u}_2(\phi_2) & \lambda_2 x_2\times\boldsymbol{u}_2'(\phi_2) & [x_3\times] & [x_4\times] \end{pmatrix}.$$

In *tame* stances, each $SII$ triplet of the four contacts gives six linearly independent columns in $D\mathcal{L}_\mathcal{K}$. Hence $D\mathcal{L}_\mathcal{K}$ has full rank on the $SSII$ cell class. In the $SSSI$ cell class, up to contact re-ordering a cell $\mathcal{K}$ has the form $\mathcal{K} = S_1 \times S_2 \times S_3 \times I_4$, and the Jacobian $D\mathcal{L}_\mathcal{K}$ is the $6 \times 9$ matrix:

$$D\mathcal{L}_\mathcal{K} = \begin{pmatrix} \boldsymbol{u}_1(\phi_1) & \lambda_1\boldsymbol{u}_1'(\phi_1) & \boldsymbol{u}_2(\phi_2) & \lambda_2\boldsymbol{u}_2'(\phi_2) & \boldsymbol{u}_3(\phi_3) & \lambda_3\boldsymbol{u}_3'(\phi_3) & I \\ x_1\times\boldsymbol{u}_1(\phi_1) & \lambda_1 x_1\times\boldsymbol{u}_1'(\phi_1) & x_2\times\boldsymbol{u}_2(\phi_2) & \lambda_2 x_2\times\boldsymbol{u}_2'(\phi_2) & x_3\times\boldsymbol{u}_3(\phi_3) & \lambda_3 x_3\times\boldsymbol{u}_3'(\phi_3) & [x_4\times] \end{pmatrix}.$$

If $\mathsf{rank}(\mathsf{D}\mathcal{L}_\mathcal{K}) = 5$ rather than full rank, $D\mathcal{L}_\mathcal{K}$ has a four-dimensional kernel in $\mathbb{R}^9$. Based on the kernel's dimensionality, the column subsets associated with *four* contact triplets must simultaneously loose their full

rank. Thus consider the column subsets associated with the contact triplets $S_1 \times S_2 \times S_3$, $S_1 \times S_2 \times I_4$, $S_1 \times S_3 \times I_4$, and $S_2 \times S_3 \times I_4$. Let $\Delta$ be the plane spanned by $x_1$, $x_2$, and $x_3$. According to Lemma .1, linear dependency of the $SSS$ columns requires that their friction cone tangent planes intersect at a common point $z \in \Delta$. Lemma .1 also states that linear dependency of each $SSI$ column subset requires that the tangent planes to the friction cones at the two $S$ contacts pass through the $I$ contact at $x_4$. These two facts imply that $\mathsf{rank}(\mathsf{D}\mathcal{L}_\mathcal{K}) = 5$ when the tangent planes to the friction cones at $x_1$, $x_2$, and $x_3$ pass through both $z$ and $x_4$. When $x_4$ lies outside $\Delta$ (which is the generic case on uneven terrains), the three tangent planes must intersect along a common line passing through $z$ and $x_4$. The case where $x_4$ lies on $\Delta$ can be treated as the limit where $x_4$ approaches $\Delta$ from the outside, and still requires that the three tangent planes intersect along a common line passing through the point $z = x_4$. The latter condition is a highly non-generic, and $D\mathcal{L}_\mathcal{K}$ therefore has full rank in the $SSSI$ cell class.

**III. Cell classes associated with five non-zero contact forces.** We have to show that $D\mathcal{L}_\mathcal{K}$ has *full rank* on the cell classes $SSSSI$, $SSSII$,...,$IIIII$. In the cell classes containing at least three $I$ contacts, $D\mathcal{L}_\mathcal{K}$ has full rank when the $I$ contacts do not lie on a common line in $\mathbb{R}^3$. In the cell class $SSSII$, the columns of $D\mathcal{L}_\mathcal{K}$ associated with any $SII$ triplet are linearly independent over *tame* stances. Hence $D\mathcal{L}_\mathcal{K}$ has full rank on the $SSSII$ cell class. In the cell class $SSSSI$, the columns of $D\mathcal{L}_\mathcal{K}$ associated with any $SSSI$ quadruplet have been shown to have full rank, therefore $D\mathcal{L}_\mathcal{K}$ has full rank on this class.

**IV. Cell classes associated with six non-zero contact forces.** All of these cell classes except $SSSSSS$ contain previously considered cell classes where $D\mathcal{L}_\mathcal{K}$ has full rank. In a cell $\mathcal{K}$ of the $SSSSSS$ class, the Jacobian $D\mathcal{L}_\mathcal{K}$ forms a $6 \times 12$ matrix. If $\mathsf{rank}(\mathsf{D}\mathcal{L}_\mathcal{K}) = 5$ rather than full rank, it has a seven-dimensional kernel in $\mathbb{R}^{12}$. Based on the kernel dimensionality, the column subsets associated with *seven* $SSS$ contact triplets must simultaneously loose their full rank. This condition can be captured by seven scalar equations associated with rank deficiency of the seven $SSS$ contact triplets. It can be verified that these constraints meet transversally in $(\phi_1, \ldots, \phi_6)$ space when the six contacts do not lie on a common plane in $\mathbb{R}^3$ (which is the generic case on uneven terrains). As the number of equations exceeds the ambient space dimension, the solution set where $\mathsf{rank}(\mathsf{D}\mathcal{L}_\mathcal{K}) = 5$ is empty, and $D\mathcal{L}_\mathcal{K}$ thus has full rank on the $SSSSSS$ cell class. When all six contacts lie on a common plane, the seven $SSS$ contact triplets specify only four independent constraints. In this special case $\mathsf{rank}(\mathsf{D}\mathcal{L}_\mathcal{K}) = 5$ is captured by three additional scalar constraints in $(\phi_1, \ldots, \phi_6)$ space, which leads to the same conclusion that $D\mathcal{L}_\mathcal{K}$ has full rank on the $SSSSSS$ cell class.

**V. Cell classes associated with $k > 6$ contacts.** All of these cell classes contain previously considered cell classes where $D\mathcal{L}_\mathcal{K}$ has full rank. These cell classes form column subsets having full rank in $D\mathcal{L}_\mathcal{K}$, which therefore has full rank on all cell classes associated with $k > 6$ contacts. □

The next proposition characterizes the critical contact forces in the cell classes listed in Theorem 2. The proposition is repeated here in a *reduced* form.

**Proposition 4.2.** *For each cell class listed in Theorem 2, the critical contact forces which are possibly mapped to the boundary of the net wrench cone $\mathcal{W}$ satisfy the following conditions.*

**1. Cell classes SI and II:** *The entire cells consist of critical contact forces. The image of these cells under $\mathcal{L}$ is a subset of a five-dimensional linear subspace of net wrenches in $\mathbb{R}^6$, which generate zero moment about the line connecting $x_1$ and $x_2$.*

**2. Cell class $SSI$:** *The cells of this class are parametrized by $(\lambda_1, \phi_1)$, $(\lambda_2, \phi_2)$, and $f_3 \in \mathbb{R}^3$. The critical contact forces satisfy the two scalar equations:*

$$\begin{array}{l} \boldsymbol{\eta}_1(\phi_1) \cdot (x_1 - x_3) = 0 \\ \boldsymbol{\eta}_2(\phi_2) \cdot (x_2 - x_3) = 0 \end{array} \tag{S.1}$$

*where $\boldsymbol{\eta}_i(\phi_i)$ is the normal to the friction cone's tangent plane $\Delta_i(\phi_i)$ for $i = 1, 2$.*

**3. Cell class $SSS$:** *The cells of this class are parametrized by $(\lambda_i, \phi_i)$ for $i = 1, 2, 3$. The critical contact forces are described by force angles $(\phi_1, \phi_2, \phi_3)$ satisfying the equation:*

$$\det \begin{bmatrix} \bar{\boldsymbol{s}} \cdot \boldsymbol{\nu}_1(\phi_1) & \bar{\boldsymbol{s}} \cdot \boldsymbol{\nu}_2(\phi_2) & \bar{\boldsymbol{s}} \cdot \boldsymbol{\nu}_3(\phi_3) \\ \bar{\boldsymbol{t}} \cdot \boldsymbol{\nu}_1(\phi_1) & \bar{\boldsymbol{t}} \cdot \boldsymbol{\nu}_2(\phi_2) & \bar{\boldsymbol{t}} \cdot \boldsymbol{\nu}_3(\phi_3) \\ \bar{\boldsymbol{n}} \cdot (x_1 \times \boldsymbol{\nu}_1(\phi_1)) & \bar{\boldsymbol{n}} \cdot (x_2 \times \boldsymbol{\nu}_2(\phi_2)) & \bar{\boldsymbol{n}} \cdot (x_3 \times \boldsymbol{\nu}_3(\phi_3)) \end{bmatrix} = 0. \tag{S.2}$$

*In this equation $\boldsymbol{\nu}_i(\phi_i) = \bar{\boldsymbol{n}} \times \boldsymbol{\eta}_i(\phi_i)$ for $i = 1, 2, 3$, where $\bar{\boldsymbol{n}}$ is the unit normal and $(\bar{\boldsymbol{s}}, \bar{\boldsymbol{t}})$ the unit tangents to the plane spanned by $x_1$, $x_2$, and $x_3$.*

**4. Cell class *SSSS*:** *The cells of this class are parametrized by* $(\lambda_i, \phi_i)$ *for* $i = 1, 2, 3, 4$. *The critical contact forces are described by angles* $(\phi_1, \phi_2, \phi_3, \phi_4)$ *satisfying three equations:*

$$\det \begin{bmatrix} \bar{\boldsymbol{s}}_i \cdot \boldsymbol{\nu}_i(\phi_i) & \bar{\boldsymbol{s}}_i \cdot \boldsymbol{\nu}_{i+1}(\phi_{i+1}) & \bar{\boldsymbol{s}}_i \cdot \boldsymbol{\nu}_{i+2}(\phi_{i+2}) \\ \bar{\boldsymbol{t}}_i \cdot \boldsymbol{\nu}_i(\phi_i) & \bar{\boldsymbol{t}}_i \cdot \boldsymbol{\nu}_{i+1}(\phi_{i+1}) & \bar{\boldsymbol{t}}_i \cdot \boldsymbol{\nu}_{i+2}(\phi_{i+2}) \\ \bar{\boldsymbol{n}}_i \cdot (x_i \times \boldsymbol{\nu}_i(\phi_i)) & \bar{\boldsymbol{n}}_i \cdot (x_{i+1} \times \boldsymbol{\nu}_{i+1}(\phi_{i+1})) & \bar{\boldsymbol{n}}_i \cdot (x_{i+2} \times \boldsymbol{\nu}_{i+2}(\phi_{i+2})) \end{bmatrix} = 0 \qquad i = 1, 2, 3 \tag{S.3}$$

*where index addition is modulo four. In these equations* $\boldsymbol{\nu}_i(\phi_i) = \bar{\boldsymbol{n}}_i \times \boldsymbol{\eta}_i(\phi_i)$, *where* $(\bar{\boldsymbol{s}}_i, \bar{\boldsymbol{t}}_i, \bar{\boldsymbol{n}}_i)$ *is a reference frame for the plane spanned by the contacts* $x_i$, $x_{i+1}$, *and* $x_{i+2}$.

**5. Cell class *SSSSS*:** *The cells of this class are parametrized by* $(\lambda_i, \phi_i)$ *for* $i = 1 \ldots 5$. *The critical contact forces are described by angles* $(\phi_1, \ldots, \phi_5)$ *satisfying five equations:*

$$\det \begin{bmatrix} \bar{\boldsymbol{s}}_i \cdot \boldsymbol{\nu}_i(\phi_i) & \bar{\boldsymbol{s}}_i \cdot \boldsymbol{\nu}_{i+1}(\phi_{i+1}) & \bar{\boldsymbol{s}}_i \cdot \boldsymbol{\nu}_{i+2}(\phi_{i+2}) \\ \bar{\boldsymbol{t}}_i \cdot \boldsymbol{\nu}_i(\phi_i) & \bar{\boldsymbol{t}}_i \cdot \boldsymbol{\nu}_{i+1}(\phi_{i+1}) & \bar{\boldsymbol{t}}_i \cdot \boldsymbol{\nu}_{i+2}(\phi_{i+2}) \\ \bar{\boldsymbol{n}}_i \cdot (x_i \times \boldsymbol{\nu}_i(\phi_i)) & \bar{\boldsymbol{n}}_i \cdot (x_{i+1} \times \boldsymbol{\nu}_{i+1}(\phi_{i+1})) & \bar{\boldsymbol{n}}_i \cdot (x_{i+2} \times \boldsymbol{\nu}_{i+2}(\phi_{i+2})) \end{bmatrix} = 0 \qquad i = 1 \ldots 5 \tag{S.4}$$

*where index addition is modulo five. In these equations* $\boldsymbol{\nu}_i(\phi_i) = \bar{\boldsymbol{n}}_i \times \boldsymbol{\eta}_i(\phi_i)$, *where* $(\bar{\boldsymbol{s}}_i, \bar{\boldsymbol{t}}_i, \bar{\boldsymbol{n}}_i)$ *is a reference frame for the plane spanned by the contacts* $x_i$, $x_{i+1}$, *and* $x_{i+2}$.

**Proof:** First consider the $SI$ cell class. The cells of this class are five-dimensional sets, hence $\mathsf{rank}(\mathsf{D}\mathcal{L}_\mathcal{K}) \leq 5$ at all points of these cells. These cells are mapped to net wrenches that generate zero torque about the line passing through $x_1$ and $x_2$. Hence their image under $\mathcal{L}$ lies in a five-dimensional subspace in $I\!R^6$. Next consider the $II$ cell class. The contact forces in a cell $\mathcal{K}$ of this class are parametrized by $(f_1, f_2) \in I\!R^6$. The Jacobian $\mathcal{L}_\mathcal{K} : I\!R^6 \to I\!R^6$ is the $6 \times 6$ matrix:

$$D\mathcal{L}_\mathcal{K} = \begin{pmatrix} I & I \\ [x_1\times] & [x_2\times] \end{pmatrix} \cong \begin{pmatrix} I & O \\ [x_1\times] & [(x_2 - x_1)\times] \end{pmatrix}$$

where $I$ is the $3 \times 3$ identity and $O$ is a $3 \times 3$ zero matrix. Noting that $\mathsf{rank}(\mathsf{D}\mathcal{L}_\mathcal{K}) = 5$ on the entire cell and that $\mathcal{L}_\mathcal{K} = D\mathcal{L}_\mathcal{K}$, the six-dimensional cell $\mathcal{K}$ is mapped by $\mathcal{L}$ to a five-dimensional set in $I\!R^6$. The wrenches in this set generate zero torque about the line passing through $x_1$ and $x_2$, and hence lie within a five-dimensional subspace of $I\!R^6$.

**Cell class SSI:** An $SSI$ cell has the form $\mathcal{K} = S_1 \times S_2 \times I_3$. Its contact forces $(f_1, f_2)$ are parametrized by $(\lambda_i, \phi_i)$ for $i = 1, 2$, while $f_3$ is parametrized by $I\!R^3$. Using these parameters, the Jacobian of $\mathcal{L}_\mathcal{K} : I\!R^7 \to I\!R^6$ is the $6 \times 7$ matrix:

$$D\mathcal{L}_\mathcal{K} = \begin{pmatrix} \boldsymbol{u}_1(\phi_1) & \lambda_1 \boldsymbol{u}_1'(\phi_1) & \boldsymbol{u}_2(\phi_2) & \lambda_2 \boldsymbol{u}_2'(\phi_2) & I \\ x_1 \times \boldsymbol{u}_1(\phi_1) & \lambda_1 x_1 \times \boldsymbol{u}_1'(\phi_1) & x_2 \times \boldsymbol{u}_2(\phi_2) & \lambda_2 x_2 \times \boldsymbol{u}_2'(\phi_2) & [x_3\times] \end{pmatrix}. \tag{S.5}$$

The columns of $D\mathcal{L}_\mathcal{K}$ associated with $x_1$ and $x_2$ span two flat pencils, which form the tangent planes $\Delta_1(\phi_1)$ and $\Delta_2(\phi_2)$, while the columns associated with $x_3$ span a solid pencil based at this point. According to Lemma .1, linear dependency of these pencils as vectors in $I\!R^6$ requires that the two flat pencils pass through the contact point $x_3$. This condition gives the two scalar equations listed in (S.1).

**Cell class SSS:** Up to contact re-ordering an $SSS$ cell has the form $\mathcal{K} = S_1 \times S_2 \times S_3$. Its contact forces $(f_1, f_2, f_3)$ are parametrized by $(\lambda_i, \phi_i)$ for $i = 1, 2, 3$. Using these parameters, the Jacobian of $\mathcal{L}_\mathcal{K} : I\!R^6 \to I\!R^6$ is the $6 \times 6$ matrix:

$$D\mathcal{L}_\mathcal{K} = \begin{pmatrix} \boldsymbol{u}_1(\phi_1) & \lambda_1 \boldsymbol{u}_1'(\phi_1) & \boldsymbol{u}_2(\phi_2) & \lambda_2 \boldsymbol{u}_2'(\phi_2) & \boldsymbol{u}_3(\phi_3) & \lambda_3 \boldsymbol{u}_3'(\phi_3) \\ x_1 \times \boldsymbol{u}_1(\phi_1) & \lambda_1 x_1 \times \boldsymbol{u}_1'(\phi_1) & x_2 \times \boldsymbol{u}_2(\phi_2) & \lambda_2 x_2 \times \boldsymbol{u}_2'(\phi_2) & x_3 \times \boldsymbol{u}_3(\phi_3) & \lambda_3 x_3 \times \boldsymbol{u}_3'(\phi_3) \end{pmatrix}.$$

The columns of $D\mathcal{L}_\mathcal{K}$ span three flat pencils which form the friction cone tangent planes $\Delta(\phi_1)$, $\Delta(\phi_2)$, and $\Delta(\phi_3)$. According to Lemma .1, these flat pencils are linearly dependent as vectors in $I\!R^6$ when they intersect at a common point located on the plane spanned by the three contacts. Let $\Delta$ denote this plane, let $\bar{\boldsymbol{n}}$ be the unit normal to $\Delta$, and let $l_i$ be the intersection line $l_i = \Delta \cap \Delta(\phi_i)$ for $i = 1, 2, 3$. The Plücker coordinates of each line $l_i$ are $(\boldsymbol{\nu}_i, x_i \times \boldsymbol{\nu}_i) \in I\!R^6$, where $\boldsymbol{\nu}_i(\phi_i) = \bar{\boldsymbol{n}} \times \boldsymbol{\eta}_i(\phi_i)$ is the direction of $l_i$. Let $(\bar{\boldsymbol{s}}, \bar{\boldsymbol{t}}, \bar{\boldsymbol{n}})$ be a reference frame for $\Delta$. A standard result from line geometry states that three co-planar lines intersect at a common point iff their Plücker coordinates with respect to this plane, $(\bar{\boldsymbol{s}} \cdot \boldsymbol{\nu}_i, \bar{\boldsymbol{t}} \cdot \boldsymbol{\nu}_i, \bar{\boldsymbol{n}} \cdot (x_i \times \boldsymbol{\nu}_i)) \in I\!R^3$, form linearly dependent vectors in $I\!R^3$:

$$\det \begin{bmatrix} \bar{\boldsymbol{s}} \cdot \boldsymbol{\nu}_1(\phi_1) & \bar{\boldsymbol{s}} \cdot \boldsymbol{\nu}_2(\phi_2) & \bar{\boldsymbol{s}} \cdot \boldsymbol{\nu}_3(\phi_3) \\ \bar{\boldsymbol{t}} \cdot \boldsymbol{\nu}_1(\phi_1) & \bar{\boldsymbol{t}} \cdot \boldsymbol{\nu}_2(\phi_2) & \bar{\boldsymbol{t}} \cdot \boldsymbol{\nu}_3(\phi_3) \\ \bar{\boldsymbol{n}} \cdot (x_1 \times \boldsymbol{\nu}_1(\phi_1)) & \bar{\boldsymbol{n}} \cdot (x_2 \times \boldsymbol{\nu}_2(\phi_2)) & \bar{\boldsymbol{n}} \cdot (x_3 \times \boldsymbol{\nu}_3(\phi_3)) \end{bmatrix} = 0. \tag{S.6}$$

This gives the scalar equation (S.2).

**Cell classes SSSS and SSSSS:** An $SSSS$ cell has the form $\mathcal{K} = S_1 \times S_2 \times S_3 \times S_4$, and its forces $(f_1, f_2, f_3, f_4)$ are parametrized by $(\lambda_i, \phi_i)$ for $i = 1, 2, 3, 4$. Using these parameters, the map $\mathcal{L}_\mathcal{K} : \mathbb{R}^8 \to \mathbb{R}^6$ has a $6 \times 8$ Jacobian whose columns form four flat pencils tangent to the friction cones at the contact points. When $\mathsf{rank}(\mathsf{D}\mathcal{L}_\mathcal{K}) = 5$, $D\mathcal{L}_\mathcal{K}$ has a three-dimensional kernel in $\mathbb{R}^8$. The kernel's dimensionality requires that *three* column subsets of $D\mathcal{L}_\mathcal{K}$ associated with three $SSS$ triplets simultaneously loose their full rank. The vanishing determinant condition (S.6) now applies to each of these $SSS$ triplets, thus giving the three scalar equations (S.3). An $SSSSS$ cell has the form $\mathcal{K} = S_1 \times \cdots \times S_5$, and its contact forces $(f_1, \ldots, f_5)$ are parametrized by $(\lambda_i, \phi_i)$ for $i = 1 \ldots 5$. Using these parameters, the map $\mathcal{L}_\mathcal{K} : \mathbb{R}^{10} \to \mathbb{R}^6$ has a $6 \times 10$ Jacobian matrix. When $\mathsf{rank}(\mathsf{D}\mathcal{L}_\mathcal{K}) = 5$, $D\mathcal{L}_\mathcal{K}$ has a five-dimensional kernel in $\mathbb{R}^{10}$. The kernel's dimensionality requires that *five* column subsets of $D\mathcal{L}_\mathcal{K}$ associated with five $SSS$ triplets simultaneously loose their full rank. The vanishing determinant condition for each $SSS$ triplet gives the five scalar equations (S.4). □

Proposition 4.2 identifies the critical contact forces in a given cell class. However, it does not ensure that these critical contact forces are mapped to the actual boundary of the net wrench cone $\mathcal{W}$. The following proposition gives additional sign conditions that describe which of these wrenches lies on the boundary of $\mathcal{W}$.

**Proposition 4.4.** *In a tame k-contact stance, for each cell class listed in Theorem 2, the critical contact forces whose image under $\mathcal{L}$ lies on the actual boundary of the net wrench cone $\mathcal{W}$ satisfy the following sign conditions.*

**1. Cell classes SI and II:** *The entire cells consist of critical contact forces. Their image under $\mathcal{L}$ lies on the boundary of $\mathcal{W}$ if and only if there exists a sign $\sigma \in \{-1, +1\}$ satisfying the inequalities:*

$$\sigma\left((x_2 - x_1) \cdot (x_i - x_1) \times n_i\right) \geq 0 \qquad i = 3 \ldots k. \tag{S.7}$$

*where $n_i$ is the terrain's unit normal at $x_i$ for $i = 3 \ldots k$. Condition (17) is automatically satisfied when the projected contacts $\tilde{x}_1, \tilde{x}_2$ are adjacent vertices of the support polygon $\mathcal{P}$.*

**2. Cell class SSI:** *The critical contact forces in this cell class are associated with fixed angles, $(\phi_1^*, \phi_2^*)$, determined by condition (12). Their image under $\mathcal{L}$ lies on the boundary of $\mathcal{W}$ if and only if there exists a sign $\sigma \in \{-1, +1\}$ satisfying the inequalities:*

$$\begin{aligned} &\sigma(\boldsymbol{\nu}^* \cdot (x_i - x_3) \times n_i \geq 0 && i{=}1{,}2 \\ &\sigma\left(\boldsymbol{\nu}^* \cdot (x_i - x_3) \times \boldsymbol{u}_i(\phi_i)\right) \geq 0 && \text{for all } \phi_i \in \mathbb{R},\ i = 4 \ldots k \end{aligned} \tag{S.8}$$

*where $\boldsymbol{\nu}^* = \boldsymbol{\eta}_1(\phi_1^*) \times \boldsymbol{\eta}_2(\phi_2^*)$ is the vector collinear with the intersection line of the tangent planes $\Delta(\phi_1^*)$ and $\Delta(\phi_2^*)$.*

**3. Cell classes SSS, SSSS, SSSSS:** *The critical contact forces in these cell classes are associated with angles $(\phi_1, \phi_2, \phi_3)$ satisfying conditions (13), (14), and (15). Let $z \in \Delta$ denote the intersection point of the friction cone tangent planes $\Delta_1(\phi_1)$, $\Delta_2(\phi_2)$, $\Delta_3(\phi_3)$, where $\Delta$ is the plane spanned by $x_1$, $x_2$, and $x_3$. The image of the critical contact forces under $\mathcal{L}$ lies on the boundary of $\mathcal{W}$ if and only if there exists a sign $\sigma \in \{-1, +1\}$ satisfying the inequalities:*

$$\begin{aligned} &\sigma\big(\bar{\boldsymbol{n}} \cdot ((x_i - z) \times \boldsymbol{\eta}_i(\phi_i))\big) \geq 0 && i = 1, 2, 3 \\ &\sigma\big(\bar{\boldsymbol{n}} \cdot \boldsymbol{u}_i(\phi_i) + \bar{\boldsymbol{\tau}} \cdot ((x_i - z) \times \boldsymbol{u}_i(\phi_i))\big) \geq 0 && \text{for all } \phi_i \in \mathbb{R},\ i = 4 \ldots k \end{aligned} \tag{S.9}$$

*where $\bar{\boldsymbol{n}}$ is the unit normal to $\Delta$, $\boldsymbol{n}_i(\phi_i)$ is normal to the tangent plane $\Delta(\phi_i)$ for $i = 1, 2, 3$, and $\bar{\boldsymbol{\tau}}(\phi_1, \phi_2, \phi_3) = [\boldsymbol{\eta}_1(\phi_1)\, \boldsymbol{\eta}_2(\phi_2)\, \boldsymbol{\eta}_3(\phi_3)]^{-1} \boldsymbol{c}$ such that $\boldsymbol{c} = (c_1, c_2, c_3)$ are the direction cosines of the tangent planes $\Delta_1(\phi_1), \Delta_2(\phi_2), \Delta_3(\phi_3)$ with respect to $\Delta$.*

**Proof:** **1. Cell classes SI and II:** Let $l_{12}$ denote the line passing through the contact points $x_1$ and $x_2$. Since the forces $(f_1, f_2)$ generate zero torque about $l_{12}$, a cell $\mathcal{K}$ of the $SI$ or $II$ cell class is mapped under $\mathcal{L}$ into a five-dimensional linear subspace, denoted $U$, in wrench space $\mathbb{R}^6$. The wrench orthogonal to $U$ in $\mathbb{R}^6$ is a pure-torque wrench about $l_{12}$. The image of the cell $\mathcal{K}$ under $\mathcal{L}$ lies on the boundary of $\mathcal{W}$ iff all contact forces $(f_1, \ldots, f_k) \in C$ generate net wrenches that lie in the *same* half-space bounded by $U$ in $\mathbb{R}^6$.

The wrenches generated by the contact forces $(f_1, f_2)$ lie within $U$. Thus consider wrenches generated by contact forces $f_i \in C_i$ for $i = 3 \ldots k$. For a *tame* stance, each friction cone $C_i$ lies above the plane spanned by the contact points $x_1$, $x_2$, and $x_i$ for $i = 3 \ldots k$. Since $l_{12}$ lies within each of these planes, all forces $f_i \in C_i$ generate the same torque sign about $l_{12}$. Hence it suffices to check the torque sign using the contact normals $n_i$ for $i = 3 \ldots k$. This gives condition (S.7).

**2. Cell class SSI:** The critical contact forces in a cell $\mathcal{K}$ of this class vary with five parameters according to Proposition 4.2, and these forces are mapped under $\mathcal{L}$ to a smooth five-dimensional manifold embedded in $I\!R^6$. Let $\boldsymbol{w}_0 \in I\!R^6$ be a particular wrench generated by critical contact forces $(f_1^0, f_2^0, f_3^0) \in S_1 \times S_2 \times I_3$, and let $V$ denote the manifold's five-dimensional tangent hyperplane at $\boldsymbol{w}_0$. The net wrench cone $\mathcal{W}$ forms a convex set in $I\!R^6$. Hence $\boldsymbol{w}_0$ lies on the boundary of $\mathcal{W}$ iff all forces $(f_1, \ldots, f_k) \in C$ generate net wrenches that lie within the *same* half-space bounded by $V$ in $I\!R^6$. The wrench orthogonal to $V$ in $I\!R^6$ is the left kernel of the Jacobian of $D\mathcal{L}_\mathcal{K}$. Selecting the origin at $x_3$ and recalling that $f_i(\lambda_i, \phi_i) = \lambda_i \boldsymbol{u}(\phi_i)$ for $i = 1, 2$, the Jacobian is the $6 \times 7$ matrix:

$$D\mathcal{L}_\mathcal{K} = \begin{pmatrix} \boldsymbol{u}_1(\phi_1^0) & \lambda_1^0 \boldsymbol{u}_1'(\phi_1^0) & \boldsymbol{u}_2(\phi_2^0) & \lambda_2^0 \boldsymbol{u}_2'(\phi_2^0) & I \\ (x_1 - x_3) \times \boldsymbol{u}_1(\phi_1^0) & \lambda_1^0 (x_1 - x_3) \times \boldsymbol{u}_1'(\phi_1^0) & (x_2 - x_3) \times \boldsymbol{u}_2(\phi_2^0) & \lambda_2^0 (x_2 - x_3) \times \boldsymbol{u}_2'(\phi_2^0) & O \end{pmatrix}$$

where $f_i^0 = \lambda_i^0 \boldsymbol{u}(\phi_i^0)$ for $i = 1, 2$, $I$ is a $3 \times 3$ identity matrix, and $O$ is a $3 \times 3$ zero matrix. The last three columns of $D\mathcal{L}_\mathcal{K}$ imply that its left kernel is spanned by the row vector $(\vec{0}, \boldsymbol{\tau}_0) \in I\!R^6$, where $\boldsymbol{\tau}_0$ is yet to be determined. The tangent plane $\Delta_i(\phi_i^0)$ for $i = 1, 2$ passes through $x_3$ according to Lemma .1. Hence the vector $x_i - x_3$ lies in $\Delta_i(\phi_i^0)$, while the vectors $(x_i - x_3) \times \boldsymbol{u}_i(\phi_i^0)$ and $(x_i - x_3) \times \boldsymbol{u}_i'(\phi_i^0)$ which appear in $D\mathcal{L}_\mathcal{K}$ are *orthogonal* to the tangent plane $\Delta_i(\phi_i^0)$ for $i = 1, 2$. The left kernel of $D\mathcal{L}_\mathcal{K}$ is therefore spanned by the row vector $(\vec{0}, \boldsymbol{\nu}^*) \in I\!R^6$, where $\boldsymbol{\nu}^* = \boldsymbol{\eta}_1(\phi_1^0) \times \boldsymbol{\eta}_2(\phi_2^0)$ is collinear with the intersection line $l = \Delta_1(\phi_1^0) \cap \Delta_2(\phi_2^0)$. Since $(\vec{0}, \boldsymbol{\nu}^*)$ is orthogonal to the subspace $V$, the half-space bounded by $V$ is given by $\{(f, \tau) \in I\!R^6 : (0, \boldsymbol{\nu}^*) \cdot (f, \tau) = \boldsymbol{\nu}^* \cdot \tau \geq 0\}$. Thus, when all net wrenches generated by the forces $(f_1, \ldots, f_k) \in C$ agree on the torque sign about $l$, these wrenches lie in the *same* half-space bounded by $V$ in $I\!R^6$. Any force $f_3 \in C_3$ generates zero torque about $l$. Since $l$ lies in the tangent plane $\Delta_i(\phi_i^0)$ for $i = 1, 2$, by convexity of $C_i$ all forces $f_i \in C_i$ automatically generate the same torque sign about $l$ for $i = 1, 2$. Hence it suffices to check the torque sign about $l$ using the contact normals $n_1$ and $n_2$. This gives the first part of (S.8). By convexity of $C_i$ for $i = 3 \ldots k$, it suffices to check the torque sign about $l$ using contact forces that lie on the friction cone boundary, $f_i = \lambda_i \boldsymbol{u}_i(\phi_i)$ for $\phi_i \in I\!R$. Since $\lambda_i > 0$, the torque sign is determined by the product $\boldsymbol{\nu}^* \cdot ((x_i - x_3) \times \boldsymbol{u}_i(\phi_i))$ for $i = 3 \ldots k$, which gives the second part of (S.8).

**3. Cell class SSS:** The critical contact forces in this cell class vary with five parameters according to Proposition 4.2, and their image under $\mathcal{L}$ forms a smooth five-dimensional manifold embedded in $I\!R^6$. Let $\boldsymbol{w}_0 \in I\!R^6$ be a particular wrench on this manifold, generated by critical contact forces $(f_1^0, f_2^0, f_3^0) \in S_1 \times S_2 \times S_3$. Let $V$ denote the manifold's tangent hyperplane at $\boldsymbol{w}_0$. The wrench orthogonal to $V$ in $I\!R^6$ is the left kernel of the $6 \times 6$ Jacobian matrix:

$$D\mathcal{L}_\mathcal{K} = \begin{pmatrix} \boldsymbol{u}_1(\phi_1^0) & \lambda_1^0 \boldsymbol{u}_1'(\phi_1^0) & \boldsymbol{u}_2(\phi_2^0) & \lambda_2^0 \boldsymbol{u}_2'(\phi_2^0) & \boldsymbol{u}_3(\phi_3^0) & \lambda_3^0 \boldsymbol{u}_3'(\phi_3^0) \\ x_1 \times \boldsymbol{u}_1(\phi_1^0) & \lambda_1^0 x_1 \times \boldsymbol{u}_1'(\phi_1^0) & x_2 \times \boldsymbol{u}_2(\phi_2^0) & \lambda_2^0 x_2 \times \boldsymbol{u}_2'(\phi_2^0) & x_3 \times \boldsymbol{u}_3(\phi_3^0) & \lambda_3^0 x_3 \times \boldsymbol{u}_3'(\phi_3^0) \end{pmatrix}$$

where $f_i^0 = \lambda_i^0 \boldsymbol{u}(\phi_i^0)$ for $i = 1, 2, 3$. Each pair $\{\boldsymbol{u}_i(\phi_i^0), \boldsymbol{u}_i'(\phi_i^0)\}$ spans the friction cone tangent plane $\Delta_i(\phi_i^0)$. The tangent planes $\Delta_1(\phi_1^0), \Delta_2(\phi_2^0), \Delta_3(\phi_3^0)$ intersect at $z \in \Delta$ according to Lemma .1, where $\Delta$ is the plane spanned by $x_1$, $x_2$, and $x_3$. Hence a suitable linear combination of $\{\boldsymbol{u}_i(\phi_i^0), \boldsymbol{u}_i'(\phi_i^0)\}$ gives the vector $x_i - z$ for $i = 1, 2, 3$. Recall that $\boldsymbol{\eta}_i(\phi_i^0)$ is normal to the tangent plane $\Delta_i(\phi_i^0)$. Another linear combination of $\{\boldsymbol{u}_i(\phi_i^0), \boldsymbol{u}_i'(\phi_i^0)\}$ gives the vector $(x_i - z) \times \boldsymbol{\eta}_i(\phi_i^0)$, which is orthogonal to $x_i - z$ within the tangent plane $\Delta_i(\phi_i^0)$. Selecting the origin at $z$, the two linear combinations can be used to represent the columns of $D\mathcal{L}_\mathcal{K}$ as

$$D\mathcal{L}_\mathcal{K} \cong \begin{pmatrix} x_1 - z & (x_1 - z) \times \boldsymbol{\eta}_1(\phi_1^0) & x_2 - z & (x_2 - z) \times \boldsymbol{\eta}_2(\phi_2^0) & x_3 - z & (x_3 - z) \times \boldsymbol{\eta}_3(\phi_3^0) \\ \vec{0} & \|x_1 - z\| \boldsymbol{\eta}_1(\phi_1^0) & \vec{0} & \|x_2 - z\| \boldsymbol{\eta}_2(\phi_2^0) & \vec{0} & \|x_3 - z\| \boldsymbol{\eta}_3(\phi_3^0) \end{pmatrix}.$$

The left kernel of $D\mathcal{L}_\mathcal{K}$ can now be determined by inspection. It is the row vector $(\bar{\boldsymbol{n}}, \bar{\boldsymbol{\tau}}) \in I\!R^6$, where $\bar{\boldsymbol{n}}$ is the unit normal to the plane $\Delta$, and $\bar{\boldsymbol{\tau}} = \left[\boldsymbol{\eta}_1(\phi_1^0)\, \boldsymbol{\eta}_2(\phi_3^0)\, \boldsymbol{\eta}_3(\phi_3^0)\right]^{-1} \boldsymbol{c}$ such that $\boldsymbol{c} = (c_1, c_2, c_3)$ are the direction cosines of the tangent planes $\Delta_1(\phi_1^0)$, $\Delta_2(\phi_2^0)$, $\Delta_3(\phi_3^0)$ with respect to the plane $\Delta$.[3]

Since $(\bar{\boldsymbol{n}}, \bar{\boldsymbol{\tau}})$ is orthogonal to the hyperplane $V$, the half-space bounded by $V$ in $I\!R^6$ is given by $\{(f, \tau) \in I\!R^6 : (\bar{\boldsymbol{n}}, \bar{\boldsymbol{\tau}}) \cdot (f, \tau) = \bar{\boldsymbol{n}} \cdot f + \bar{\boldsymbol{\tau}} \cdot \tau \geq 0\}$. It follows that $\boldsymbol{w}_0$ lies on the boundary of $\mathcal{W}$ iff all contact forces

[3] The direction cosines are given by $c_i = \bar{\boldsymbol{n}} \cdot ((x_i - z) \times \boldsymbol{\eta}_i)) / \|x_i - z\| \|\boldsymbol{\eta}_i\|$ for $i = 1, 2, 3$.

$(f_1,\ldots,f_k)\in C$ satisfy the inequality:

$$\bar{\boldsymbol{n}}\cdot f_i+\bar{\boldsymbol{\tau}}\cdot(x_i-z)\times f_i\geq 0 \qquad f_i\in C_i \text{ for } i=1\ldots k. \tag{S.10}$$

Condition (S.10) is simplified below for $f_i\in C_i$ such that $i=1,2,3$. For $f_i\in C_i$ such that $i=4\ldots k$, by convexity of each $C_i$ it suffices to check condition (S.10) using contact forces that lie on the friction cone's boundary, $f_i=\lambda_i\boldsymbol{u}_i(\phi_i)$ for $\phi_i\in I\!R$. This gives the second part of condition (19).

To simplify condition (S.10) for $f_i\in C_i$ such that $i=1,2,3$, recall that $\boldsymbol{\eta}_i(\phi_i^0)$ is normal to the tangent plane $\Delta_i(\phi_i^0)$. Let $\bar{\boldsymbol{\eta}}_i$ denote the projection of $\boldsymbol{\eta}_i(\phi_i^0)$ to the plane $\Delta$, $\bar{\boldsymbol{\eta}}_i=[I-\bar{\boldsymbol{n}}\bar{\boldsymbol{n}}^T]\boldsymbol{\eta}_i(\phi_i^0)$ for $i=1,2,3$. Any local variation $f_i^0+\Delta f_i\in C_i$ can be written as $\Delta f_i=\Delta f_{i1}+\Delta f_{i2}$, such that $\Delta f_{i1}$ is tangent to $S_i$ at $f_i^0$ while $\Delta f_{i2}=\kappa_i\bar{\boldsymbol{\eta}}_i$ for some $\kappa_i\geq 0$. By convexity of $C_i$, when all wrenches generated by $f_i^0+\Delta f_i\in C_i$ lie in the same half-space bounded by $V$, all forces $f_i\in C_i$ are mapped under $\mathcal{L}$ into this half-space in $I\!R^6$. The wrench generated by $f_i^0+\Delta f_{i1}$ is spanned by the two columns of $D\mathcal{L}_{\mathcal{K}}$ associated with the contact point $x_i$. This wrench is orthogonal to the left kernel $(\bar{\boldsymbol{n}},\bar{\boldsymbol{\tau}})$ of $D\mathcal{L}_{\mathcal{K}}$. The wrench generated by $\Delta f_{i2}=\kappa_i\bar{\boldsymbol{\eta}}_i$ satisfies $(\bar{\boldsymbol{n}},\bar{\boldsymbol{\tau}})\cdot(\Delta f_{i2},(x_i-z)\times\Delta f_{i2})=\kappa_i\,\bar{\boldsymbol{\tau}}\cdot((x_i-z)\times\bar{\boldsymbol{\eta}}_i)$, where we used the fact that $\bar{\boldsymbol{n}}\cdot\bar{\boldsymbol{\eta}}_i=0$. The vector $(x_i-z)\times\bar{\boldsymbol{\eta}}_i$ is collinear with $\bar{\boldsymbol{n}}$. Hence $\kappa_i\,\bar{\boldsymbol{\tau}}\cdot((x_i-z)\times\bar{\boldsymbol{\eta}}_i)=\kappa_i\,(\bar{\boldsymbol{\tau}}\cdot\bar{\boldsymbol{n}})\bar{\boldsymbol{n}}\cdot((x_i-z)\times\bar{\boldsymbol{\eta}}_i)$. Finally $\bar{\boldsymbol{n}}\times\bar{\boldsymbol{\eta}}_i=\bar{\boldsymbol{n}}\times\boldsymbol{\eta}_i$, so we can use $\boldsymbol{\eta}_i$ rather than its projection $\bar{\boldsymbol{\eta}}_i$. Thus, all local force variations $f_i^0+\Delta f_i\in C_i$ (and hence all forces $f_i\in C_i$) generate net wrenches in the half-space bounded by $V$ satisfying the inequality $\kappa_i(\bar{\boldsymbol{\tau}}\cdot\bar{\boldsymbol{n}})\,\bar{\boldsymbol{n}}\cdot((x_i-z)\times\boldsymbol{\eta}_i)\geq 0$. This inequality must hold for $i=1,2,3$. The sign of these inequalities is not affected by $\kappa_1,\kappa_2,\kappa_3\geq 0$ or by the common factor $\bar{\boldsymbol{\tau}}\cdot\bar{\boldsymbol{n}}$. This gives the first part of condition (19).

**4. Cell classes SSSS and SSSSS:** The critical contact forces in these cell classes vary with five parameters according to Proposition 4.2, and their image under $\mathcal{L}$ forms a smooth five-dimensional manifold embedded in $I\!R^6$. Let $\boldsymbol{w}_0\in I\!R^6$ be a particular wrench on this manifold, generated by critical contact forces in the respective cell class. Let $V$ denote the manifold's tangent hyperplane at $\boldsymbol{w}_0$. The wrench orthogonal to $V$ in $I\!R^6$ is the left kernel of the Jacobian matrix $D\mathcal{L}_{\mathcal{K}}$, which is $6\times 8$ in the $SSSS$ cell class and $6\times 10$ in the $SSSSS$ cell class. Since the columns associated with any $SSS$ triplet must be linearly dependent, we may compute the left kernel of $D\mathcal{L}_{\mathcal{K}}$ using the columns associated with the contacts $x_1$, $x_2$, and $x_3$. This gives the same left kernel, $(\bar{\boldsymbol{n}},\bar{\boldsymbol{\tau}})\in I\!R^6$, computed for the $SSS$ cell class. Hence one may use the same condition (19) for the $SSS$, $SSSS$, and $SSSSS$ cell classes. □

Theorem 3 which is repeated here in a *reduced* form describes the five types of boundary curves of the feasible equilibrium region $\widetilde{\mathcal{R}}$.

**Theorem 3.** *In a tame k-contact stance, the horizontal cross-section of the feasible equilibrium region, $\widetilde{\mathcal{R}}\subset I\!R^2$, is bounded by up to* **five types** *of curves:*

*1.* **SI/II segment:** *A* **linear segment** *which lies on the support polygon edge connecting the projected contacts $\tilde{x}_1$ and $\tilde{x}_2$ in $I\!R^2$.*

*2.* **SSI segment:** *A* **linear segment** *that lies on the horizontal projection of the intersection line of the friction cone tangent planes $\Delta_1(\phi_1^*)$ and $\Delta_2(\phi_2^*)$.*

*3.* **SSS curve:** *The contact forces satisfy the scalar equation (13) combined with the scalar equation:*

$$\det\begin{bmatrix}\mathbf{E}\boldsymbol{u}_1(\phi_1) & \mathbf{E}\boldsymbol{u}_2(\phi_2) & \mathbf{E}\boldsymbol{u}_3(\phi_3)\\ \boldsymbol{e}\cdot(x_1\times\boldsymbol{u}_1(\phi_1)) & \boldsymbol{e}\cdot(x_2\times\boldsymbol{u}_2(\phi_2)) & \boldsymbol{e}\cdot(x_3\times\boldsymbol{u}_3(\phi_3))\end{bmatrix}=0. \tag{S.11}$$

*The contact force angles $(\phi_1,\phi_2,\phi_3)$ form a one-dimensional solution set which maps to a* **convex arc** *on the boundary of $\widetilde{\mathcal{R}}$.*

*4.* **SSSS curve:** *The contact forces satisfy (14) as well as the separation condition (19). The contact force angles $(\phi_1,\phi_2,\phi_3,\phi_4)$ form a one-dimensional solution set which maps to a* **convex arc** *on the boundary of $\widetilde{\mathcal{R}}$.*

*5.* **SSSSS segment:** *Each solution $(\phi_1^*,\ldots,\phi_5^*)$ of (15) determines a* **linear segment** *on the boundary of $\widetilde{\mathcal{R}}$.*

**Proof:** We have to consider the intersection $\mathsf{bdy}(\mathcal{W})\cap L$ for each cell class specified in Theorem 2. The $SI$ and $II$ cell classes are associated with two non-zero contact forces. These forces can possibly balance the gravitational force only when $\mathcal{B}$'s center of mass lies in the vertical plane containing the contact points $x_1$ and $x_2$. The horizontal cross-section of this vertical plane gives a line passing through the projected contacts

$\tilde{x}_1$ and $\tilde{x}_2$ in $I\!R^2$. Since $\widetilde{\mathcal{R}}$ is a bounded convex set for *tame* stances, this line contributes a linear segment to the boundary of $\widetilde{\mathcal{R}}$.

In the $SSI$ cell class, the contact forces are parametrized by $f_i = \lambda_i \boldsymbol{u}_i(\phi_i)$ for $i = 1, 2$ while $f_3 \in I\!R^3$. The critical contact forces in an $SSI$ cell satisfy (12), which gives a finite number of solutions, $(\phi_1^*, \phi_2^*)$. These angles are held fixed while the magnitudes $\lambda_1, \lambda_2 > 0$ and $f_3$ vary freely within the cell. The intersection $\mathsf{bdy}(\mathcal{W}) \cap L$ can now be computed by solving parts (I) and (II) of the equilibrium stance equation in the unknowns $\lambda_1$, $\lambda_2$, and $f_3$:

$$\begin{aligned} &\lambda_1 \boldsymbol{u}_1(\phi_1^*) + \lambda_2 \boldsymbol{u}_2(\phi_2^*) + f_3 = \boldsymbol{e} \\ &\boldsymbol{e} \cdot (\lambda_1 x_1 \times \boldsymbol{u}_1(\phi_1^*) + \lambda_2 x_2 \times \boldsymbol{u}_1(\phi_1^*) + x_3 \times f_3) = 0. \end{aligned} \tag{S.12}$$

The solution of (S.12) forms an affine line in $(\lambda_1, \lambda_2, f_3)$ space. The image of this line under the linear map (21) gives a line in $I\!R^2$. Since $\widetilde{\mathcal{R}}$ is a bounded convex set for *tame* stances, this line contributes a linear segment to the boundary of $\widetilde{\mathcal{R}}$. Geometrically, the three contact forces intersect the line $l = \Delta_1(\phi_1^*) \cap \Delta_2(\phi_2^*)$, and therefore generate zero torque about this line. Since the gravitational force must generate zero torque about $l$ to maintain the equilibrium stance, $\boldsymbol{x}_c$ must lie in the vertical plane containing this line. The horizontal cross-section of this vertical plane gives the line which contains the $SSI$ boundary segment of $\widetilde{\mathcal{R}}$.

In the $SSS$ cell class, the contact forces are parametrized by $f_i = \lambda_i \boldsymbol{u}_i(\phi_i)$ for $i = 1, 2, 3$. The critical contact forces in an $SSS$ cell satisfy the scalar equation (13) in $(\phi_1, \phi_2, \phi_3)$, while the magnitudes $\lambda_1, \lambda_2, \lambda_3 > 0$ vary freely within the cell. The magnitudes $\lambda_1, \lambda_2, \lambda_3$ are determined by the horizontal force balance in part (I) and the torque balance about $\boldsymbol{e}$ in part (II) of the equilibrium stance equation:

$$\begin{bmatrix} \mathbf{E}\boldsymbol{u}_1(\phi_1) & \mathbf{E}\boldsymbol{u}_2(\phi_2) & \mathbf{E}\boldsymbol{u}_3(\phi_3) \\ \boldsymbol{e}\cdot(x_1 \times \boldsymbol{u}_1(\phi_1)) & \boldsymbol{e}\cdot(x_2 \times \boldsymbol{u}_2(\phi_2)) & \boldsymbol{e}\cdot(x_3 \times \boldsymbol{u}_3(\phi_3)) \end{bmatrix} \begin{pmatrix} \lambda_1 \\ \lambda_2 \\ \lambda_3 \end{pmatrix} = \begin{pmatrix} 0 \\ 0 \\ 0 \end{pmatrix}. \tag{S.13}$$

Since (S.13) must be satisfied for $\lambda_1, \lambda_2, \lambda_3 > 0$, the determinant of the $3 \times 3$ matrix in (S.13) must vanish. This gives the scalar equation (S.11). The combined solution of (13) and (S.11) forms a one-dimensional solution set in $(\phi_1, \phi_2, \phi_3)$ space. The force magnitudes corresponding to this solution set are determined by part (I) of the equilibrium stance equation, $\lambda_1 \boldsymbol{u}_1(\phi_1) + \lambda_2 \boldsymbol{u}_2(\phi_2) + \lambda_3 \boldsymbol{u}_3(\phi_3) = \boldsymbol{e}$, and the image of the resulting contact forces under the linear map (21) gives the nonlinear boundary curve of $\widetilde{\mathcal{R}}$.

The geometric interpretation of (22) is based on line geometry. The Plücker coordinates of the contact force lines are given by $(\boldsymbol{u}_i(\phi_i), x_i \times \boldsymbol{u}_i(\phi_i)) \in I\!R^6$ for $i = 1, 2, 3$. The Plücker components of the force lines with respect to the horizontal $(x, y)$ plane are given by $(\mathbf{E}\boldsymbol{u}_i(\phi_i), \boldsymbol{e} \cdot (x_i \times \boldsymbol{u}_i(\phi_i)) \in I\!R^3$ for $i = 1, 2, 3$. A standard result from line geometry states that three co-planar lines intersect at a common point iff their Plücker components with respect to the plane form linearly dependent vectors in $I\!R^3$. The vanishing determinant in (S.13) implies that the horizontal projection of the contact force lines intersect at a common point in $I\!R^2$. The three contact force lines must therefore intersect a common vertical line in $I\!R^3$.

In the $SSSS$ cell class, the contact forces are parametrized by $f_i = \lambda_i \boldsymbol{u}_i(\phi_i)$ for $i = 1, 2, 3, 4$. The critical contact forces in this class satisfy the three scalar equations (14) in $(\phi_1, \phi_2, \phi_3, \phi_4)$, whose solution forms a one-dimensional set in $(\phi_1, \phi_2, \phi_3, \phi_4)$ space. The force magnitudes corresponding to each solution $(\phi_1, \phi_2, \phi_3, \phi_4)$ are determined by the $4 \times 4$ linear system consisting of part (I) and the torque balance about $\boldsymbol{e}$ in part (II) of the equilibrium stance equation:

$$\begin{aligned} &\lambda_1 \boldsymbol{u}_1(\phi_1) + \lambda_2 \boldsymbol{u}_2(\phi_2) + \lambda_3 \boldsymbol{u}_3(\phi_3) + \lambda_4 \boldsymbol{u}_4(\phi_4) = \boldsymbol{e} \\ &\boldsymbol{e} \cdot \big(\lambda_1 x_1 \times \boldsymbol{u}_1(\phi_1) + \lambda_2 x_2 \times \boldsymbol{u}_2(\phi_2) + \lambda_3 x_3 \times \boldsymbol{u}_3(\phi_3) + \lambda_4 x_4 \times \boldsymbol{u}_4(\phi_4)\big) = 0. \end{aligned} \tag{S.14}$$

Solutions of (S.14) satisfying $\lambda_1, \lambda_2, \lambda_3, \lambda_4 > 0$ contribute points $\tilde{\boldsymbol{x}}_c$ on the boundary of $\widetilde{\mathcal{R}}$, determined by part (III) of the equilibrium stance equation:

$$\tilde{\boldsymbol{x}}_c = -\mathbf{E}\left(\boldsymbol{e} \times \textstyle\sum_{i=1}^4 \lambda_i(\boldsymbol{\phi})\, x_i \times \boldsymbol{u}_i(\phi_i)\right) \qquad \boldsymbol{\phi} = (\phi_1, \phi_2, \phi_3, \phi_4)$$

where $\boldsymbol{\phi} = (\phi_1, \phi_2, \phi_3, \phi_4)$ varies along the one-dimensional solution set of (14).

Finally consider the $SSSSS$ cell class. Its contact forces are parametrized by $f_i = \lambda_i \boldsymbol{u}_i(\phi_i)$ for $i = 1, \ldots, 5$. The critical contact forces in this class satisfy the five scalar equations (15) in $(\phi_1, \ldots, \phi_5)$. These

equations give a finite number of solutions, $(\phi_1^*, \ldots, \phi_5^*)$. The force magnitudes associated with each particular solution are obtained by solving the $4\times5$ linear system in $\lambda_1, \ldots, \lambda_5$:

$$\begin{aligned} &\lambda_1 \boldsymbol{u}_1(\phi_1^*) + \cdots + \lambda_5 \boldsymbol{u}_5(\phi_5^*) = \boldsymbol{e} \\ &\boldsymbol{e} \cdot \big(\lambda_1 x_1 \times \boldsymbol{u}_1(\phi_1^*) + \cdots + \lambda_5 x_5 \times \boldsymbol{u}_5(\phi_5^*)\big) = 0. \end{aligned} \tag{S.15}$$

The solution of (S.15) forms an affine line in $(\lambda_1, \ldots, \lambda_5)$ space. The portion of this affine line satisfying $\lambda_1, \ldots, \lambda_5 > 0$ contributes a linear segment to the boundary of $\widetilde{\mathcal{R}}$ via part (III) of the equilibrium stance equation:

$$\tilde{\boldsymbol{x}}_c = -\mathbf{E}\left(\boldsymbol{e} \times \textstyle\sum_{i=1}^5 \lambda_i(\boldsymbol{\phi}^*)\, x_i \times \boldsymbol{u}_i(\phi_i^*)\right) \qquad \boldsymbol{\phi}^* = (\phi_1^*, \ldots, \phi_5^*)$$

To compute the line containing an $SSSSS$ boundary segment, consider the left kernel, $(\boldsymbol{s}, \boldsymbol{t}) \in I\!R^6$, of the $6\times5$ matrix whose columns represent the wrenches generated by the contact forces:

$$(\boldsymbol{s}, \boldsymbol{t}) \begin{bmatrix} \boldsymbol{u}_1(\phi_1^*) & \boldsymbol{u}_2(\phi_2^*) & \boldsymbol{u}_3(\phi_3^*) & \boldsymbol{u}_4(\phi_4^*) & \boldsymbol{u}_5(\phi_5^*) \\ x_1 \times \boldsymbol{u}_1(\phi_1^*) & x_2 \times \boldsymbol{u}_2(\phi_2^*) & x_3 \times \boldsymbol{u}_3(\phi_3^*) & x_4 \times \boldsymbol{u}_4(\phi_4^*) & x_5 \times \boldsymbol{u}_5(\phi_5^*) \end{bmatrix} = (\vec{0}, \vec{0}).$$

When the net wrench generated by the contact forces balances the gravitational wrench acting on $\mathcal{B}$, a positive linear combination of the columns of the $6\times5$ matrix is collinear with the gravitational wrench, $(\boldsymbol{e}, \boldsymbol{x}_c \times \boldsymbol{e})$, acting on $\mathcal{B}$.[4] The left kernel must therefore be orthogonal to the gravitational wrench, thus giving the linear equation: $(\boldsymbol{s}, \boldsymbol{t}) \cdot (\boldsymbol{e}, \boldsymbol{x}_c \times \boldsymbol{e}) = \boldsymbol{x}_c \cdot (\boldsymbol{e} \times \boldsymbol{t}) + \boldsymbol{e} \cdot \boldsymbol{s} = 0$. This equation specifies a vertical plane for $\boldsymbol{x}_c$ in $I\!R^3$, which determines the horizontal line containing the $SSSSS$ boundary segment of $\widetilde{\mathcal{R}}$. □

[4] Recall that the contact forces are scaled such that $\|f_g\| = 1$.